Redox Biology 75 (2024) 103244

Contents lists available at ScienceDirect

Redox Biology

journal homepage: www.elsevier.com/locate/redox

A detrimental role of endothelial S1PR2 in cardiac ischemia-reperfusion injury via modulating mitochondrial dysfunction, NLRP3 inflammasome activation, and pyroptosis

Yunhao Duan [a,1], Qinyu Li [b,1], Jinjin Wu [c,1], Caixia Zhou [a], Xiuxiang Liu [a], Jinnan Yue [a], Xiaoli Chen [a], Jie Liu [a], Qi Zhang [d,**], Yuzhen Zhang [a,***], Lin Zhang [a,e,*]

[a] State Key Laboratory of Cardiovascular Diseases and Medical Innovation Center, Shanghai East Hospital, School of Medicine, Tongji University, Shanghai, 200120, China
[b] Department of Clinical Laboratory, Gongli Hospital of Shanghai Pudong New Area, 219 Miao Pu Road, Shanghai, 200135, China
[c] Department of Cardiology, Shanghai Children's Medical Center, Shanghai Jiao Tong University School of Medicine, Shanghai, 200127, China
[d] Department of Cardiology, Shanghai East Hospital, Tongji University School of Medicine, Shanghai, 200120, China
[e] Clinical Center for Heart Disease Research, School of Medicine, Tongji University, Shanghai, China

ARTICLE INFO

Keywords:
S1pr2
Endothelial cells
Cardiac I/R
Mitochondria
Inflammasome
Pyroptosis

ABSTRACT

Sphingosine 1-phosphate (S1P), a bioactive lipid molecule, exerts multifaceted effects on cardiovascular functions via S1P receptors, but its effects on cardiac I/R injury are not fully understood. Plasma lipidomics analysis by mass spectrometry revealed that sphingosine lipids, including sphingosine 1-phosphate (S1P), were significantly down-regulated following cardiac I/R injury in mice. The reduced S1P levels were also observed in the plasma of coronary heart disease (CHD) patients after percutaneous coronary intervention (PCI) compared with those without PCI. We found that S1P exerted a cardioprotective effect via endothelial cell (EC)-S1PR1, whereas EC-S1PR2 displayed a detrimental effect on cardiac I/R. Our data showed that EC-specific *S1pr2* loss-of-function significantly lessened inflammatory responses and diminished cardiac I/R injury, while EC-specific *S1pr2* gain-of-function aggravated cardiac I/R injury. Mechanistically, EC-S1PR2 initiated excessive mitochondrial fission and elevated ROS production via RHO/ROCK1/DRP1 pathway, leading to NLRP3 inflammasome activation and subsequent cell pyroptosis, thereby exacerbating inflammation and I/R injuries. Furthermore, RGD-peptide magnetic nanoparticles packaging *S1pr2-siRNA* to specifically knockdown S1PR2 in endothelial cells significantly ameliorated cardiac I/R injury. Taken together, our investigations demonstrate that EC-S1PR2 induces excessive mitochondrial fission, which results in NLRP3 inflammasome activation and subsequently triggers cell pyroptosis, ultimately exacerbating inflammatory responses and aggravating heart injuries following I/R.

1. Introduction

As the key treatment for myocardial infarction (MI), reperfusion therapy, including percutaneous coronary intervention (PCI) and fibrinolytic therapy, promptly restores coronary blood flow in the ischemic heart and limits infarct size. Paradoxically, the restoration of blood supply to the ischemic myocardium can cause additional cardiac damage, which is referred to as cardiac ischemia-reperfusion (I/R) injury [1]. This additional cardiac injury not only reduces the beneficial effects of reperfusion interventions, but also aggravates the morbidity and mortality associated with MI [2]. Therefore, it is urgent to clarify the detailed molecular mechanisms that underlie pathological cardiac remodeling after cardiac I/R injury.

* Corresponding author. State Key Laboratory of Cardiovascular Diseases and Medical Innovation Center, Shanghai East Hospital, School of Medicine, Tongji University, 150 Jimo Rd, Pudong New District, Shanghai, 200120, China.
** Corresponding author. Department of Cardiology Shanghai East Hospital, Tongji University School of Medicine 150 Jimo Rd, Pudong New District, Shanghai, 200120, China.
*** Corresponding author. State Key Laboratory of Cardiovascular Diseases and Medical Innovation Center, Shanghai East Hospital, School of Medicine, Tongji University, 150 Jimo Rd, Pudong New District, Shanghai, 200120, China.
E-mail addresses: zhangqnh@hotmail.com (Q. Zhang), yzzhang-tj@tongji.edu.cn (Y. Zhang), zhanglin1209@tongji.edu.cn (L. Zhang).
[1] These authors contributed equally to this work.

https://doi.org/10.1016/j.redox.2024.103244
Received 17 May 2024; Received in revised form 11 June 2024; Accepted 17 June 2024
Available online 19 June 2024

Abbreviations:

S1P	sphingosine 1-phosphate
S1pr2	sphingosine 1-phosphate receptor 2
ECs	endothelial cells
I/R	ischemia-reperfusion
TTC	triphenyltetrazolium chloride
DOP	4-deoxypyridoxine
CMVECs	mouse cardiac microvascular endothelial cells
mtDNA	mitochondrial DNA
mPTP	mitochondrial permeability transition pore

In contrast to the extensive investigations on cardiomyocyte I/R injury [2], the effect of microvascular dysfunctions during the process of cardiac I/R remains relatively unelucidated [3]. Previous investigations suggest that endothelial cell dysfunction significantly contributes to the development of cardiac ischemia-reperfusion injury [4,5]. Upon restoration of blood flow during reperfusion in ischemic myocardium, the endothelial dysfunctions, impaired barrier function and local inflammatory responses in cardiac endothelial cells (ECs), which exacerbates the cardiac injury following myocardial reperfusion [6,7]. Mitochondria dynamics is essential for the cellular responses towards extracellular stimuli and the maintenance of EC functional integrity [8]. When myocardial blood perfusion is restricted, a reduced energy metabolism leads to an increase in mitochondrial amount by the activation of mitochondrial fission to meet cellular metabolic demands [9]. However, under pathological conditions, this excessive mitochondrial fission can result in mitochondrial damage [10], which impairs mitochondrial redox homeostasis, increases oxidative stress, decreases mitochondrial membrane potential, elevates mitochondrial permeability and triggers mitochondrial DNA (mtDNA) leakage into cytoplasm [11]. In these circumstances, mitochondria shift from their role as "power generators" to that of "inducers of cell apoptosis or death" [12]. It has been shown that the extracellular release of mtDNA can trigger inflammasome activation [13], which may lead to cell pyroptosis, a distinct form of inflammatory cell death [14]. However, it has not been clarified whether I/R-induced mitochondria damages in ECs can trigger inflammasome activation and cause subsequent pyroptosis, eventually exacerbating cardiac I/R injury.

Sphingosine 1-phosphate (S1P), a bioactive lipid molecule, is an important regulator in cardiovascular development and functions [15]. S1P exerts its regulatory effects via a family of five G protein-coupled receptors, including S1PR1, S1PR2, S1PR3, S1PR4 and S1PR5, and thus exhibits a spectrum of diverse and multifaceted biological functions [16]. Our previous studies demonstrated that S1PR1, S1PR2, and S1PR3 were the major S1P receptor subtypes in cardiac tissues [17]. It has been documented that S1P exerted its cardioprotective effects via S1PR1 signaling, while S1PR2 disturbed endothelial dysfunctions and might exhibit detrimental effects on heart [18]. However, whether EC-expressing S1PR2 is involved in the process of cardiac I/R injury remains completely unknown.

Herein, we demonstrated that EC-specific S1PR2 deletion alleviated inflammatory responses and cardiac I/R injuries, while S1PR2 overexpression in ECs aggravated cardiac inflammation and injuries *in vivo*. Mechanistically, S1PR2 induced EC mitochondrial hyperfission via RHO/ROCK1/DRP1 pathway, thereby initiating NLRP3 inflammasome activation which in turn induced cell pyroptosis, ultimately exacerbating inflammatory responses and worsening heart injuries induced by I/R. Moreover, we constructed RGD-peptide magnetic nanoparticles packaging *S1pr2-siRNA* to specifically knockdown S1PR2 in ECs, which significantly ameliorated cardiac I/R injuries *in vivo*, providing a future promising EC-target therapy for heart I/R injury through the S1PR2 signal pathway.

2. Methods

2.1. Animals

The conditional *S1pr2* loss-of-function ($S1pr2^{flox/flox}$) mouse was generated by flanking exon 2 with loxP sites in *S1pr2* genomic DNA and the $S1pr2^{Tg/Wt}$ mouse was generated by inserting a *S1pr2*-3Xflag-IRES-EGFP cassette into the *Rosa26* locus. The conditional *S1pr2* loss-of-function ($S1pr2^{flox/flox}$) and gain-of-function ($S1pr2^{Tg/WT}$) mice were crossed with tamoxifen-inducible *VECadherin* promoter-driven *Cre* line ($VECadherin\text{-}Cre^{ERT2}$) to generate endothelial cells (ECs)-specific *S1pr2* loss- and gain-of-function mice, $S1pr2^{ECKO}$ and $S1pr2^{ECTg}$, respectively. The *Nlrp3* conditional loss-of-function mice ($Nlrp3^{flox/flox}$) were described previously [19]. The $Nlrp3^{flox/flox}$ mice were crossed with $S1pr2^{Tg/WT}$ mice to generate EC *S1pr2* overexpression and *Nlrp3* knockout mice. All strains were crossed on a C57BL/6 background. All animals were housed in a pathogen-free facility. Before the experiment, animals were anesthetized through intraperitoneal injection of pentobarbital sodium (50 mg/kg, *i.p.*). At the end of the experiment, mice were euthanized through an anesthetic overdose of pentobarbital sodium (150 mg/kg, *i.p.*) followed by cervical dislocation. All experiments were performed in accordance with the guidelines from the National Institutes of Health (NIH) Guide for the Care and Use of Laboratory Animals and approved by the University Committee on Animal Care of Tongji University with license number TJBB00223103.

2.2. Tamoxifen administration

Tamoxifen (#T5648, Sigma, USA) was dissolved in corn oil (#C67366, ABCONE, China), and administered at 100 mg/kg via intraperitoneally (*i.p.*) injection every other day for a total of 4 injections in adult mice.

2.3. Human blood samples

Human plasma samples were acquired from the Shanghai East Hospital affiliated Tongji University, School of Medicine. Peripheral blood samples were collected from patients with unstable angina (UA, n = 17) 24 h after undergoing coronary angiography (CAG). Additional samples were obtained from patients diagnosed with UA (n = 5) or ST-segment elevation myocardial infarction (STEMI, n = 23) 24 h after undergoing either elective percutaneous coronary intervention (PCI) for UA or emergency PCI for STEMI. The detailed information of the patients was presented in Supplementary Table 1. Blood samples were placed in sodium citrate treated anticoagulant tubes at room temperature (RT) and centrifugation at 1000×*g* for 15 min. Plasma samples were aliquoted and stored at −80 °C. The S1P concentrations in plasma were measured by S1P ELISA kit (#K-1900, Echelon Biosciences, USA). The study was conducted in accordance with the Declaration of Helsinki principles and the International Council for Harmonization Guidelines on Good Clinical Practice. Before the collection of samples, informed consent was obtained from each patient. The use of human peripheral blood samples for research was approved by Shanghai East Hospital's Institutional Review Board (IRB protocol number: 2021-025).

2.4. Tie2-promoter-driven adeno-associated virus 9 (AAV9) for knockdown of Gsdmd in endothelial cells

AAV9-Tie2-Gsdmd shRNA and *AAV9-Tie2-scramble* (negative control) viruses were designed by Hanbio Biotechnology (Shanghai, China). The *AAV9-Tie2-Gsdmd shRNA* was engineered to specifically target and knockdown the *Gsdmd* gene expression in endothelial cells (Supplementary Table 2). A total volume of 150 μl containing *AAV9-Tie2-Gsdmd shRNA* at a concentration of 1.5×10^{12} vg/mL viral genomes or *AAV9-Tie2-scramble* was intravenously injected through the tail vein of mice. This administration was performed two weeks prior to cardiac I/R

procedure.

2.5. RGD-peptide magnetic nanoparticles (NP) target delivery of S1pr2-siRNA

The targeted delivery of *S1pr2-siRNA* to endothelial cells (ECs) using RGD-peptide magnetic nanoparticles was performed according to a previously described method with certain modifications [18,20]. In brief, synthetic mouse *S1pr2-siRNA* or *scramble-siRNA* (GenePharma, China) was combined with RGD-peptide-coated Fe_3O_4 magnetic nanoparticles (NPs) at a ratio of 10 μg siRNA to 50 μg nanoparticles in 100 μl of normal saline at room temperature (Supplementary Table 2). This mixture was allowed to incubate for 1 h, enabling the siRNA to be encapsulated within the internal space of the NPs. The RGD-peptide magnetic nanoparticles at a dose of 2 mg/kg loaded with either *S1pr2-siRNA* or *scramble-siRNA* were administered via tail vein injection, accompanied by the placement of a magnet on the left chest. This administration was carried out twice a week for a duration of 2 weeks before I/R surgery.

2.6. The induction of heart ischemia-reperfusion animal models

For anesthesia, pentobarbital sodium (50 mg/kg, *i.p.*) was performed. Subsequently, the animals were mechanically ventilated with 1–2% vol/vol isoflurane using a rodent respirator device (ALC-V8S, ALCBIO, China). A left thoracic incision was made to expose the heart, and myocardial ischemia was induced by placing a slipknot around the left anterior descending coronary artery using a 6-0 silk suture. The slipknot was released after 45 min to allow reperfusion, and the duration of reperfusion varied based on the specific experimental objectives. A reperfusion time of 6 h was used to investigate the levels of S1P concentration in plasma and *S1pr2* expression in heart tissues or in heart endothelial cells. A reperfusion time of 24 h was used to analyze infarct size performed by evans blue/2,3,5-triphenyltetrazolium chloride (TTC) staining of heart sections. And sham-operated mice were performed with only a left thoracic incision. After recovery, repeat analgesic administration was given with carprofen (10 mg/kg) every 24 h and buprenorphine (0.1 mg/kg) every 12 h for 48 h. In pharmacological experiments, for S1P lyase THI (2-Acetyl-5-tetrahydroxybutyl Imidazole) (#13222, Cayman Chemical, USA) treatment mice, THI was dissolved in water containing 10 g/L glucose. C57BL/6 mice, aged 6–8 weeks and weighing 20–25 g, were administered THI at a dosage of 10 μg per mouse. This treatment was given twice daily for three days before the heart ischemia-reperfusion model and during the heart ischemia-reperfusion injury process, via oral gavage in a volume of 100 μl. Control mice received an equivalent volume of the solvent alone. For S1P lyase inhibitor 4-deoxypyridoxine (DOP) (#D0501, Sigma-Aldrich (Shanghai) Trading Co. Ltd) treatment mice, DOP was administered at a concentration of 30 mg/L via drinking water per day for 7 days prior to the I/R surgery, aiming to elevate S1P concentrations, and DMSO as a control, through intraperitoneal (*i.p.*) injections per day for 7 days prior to the cardiac I/R surgery.

2.7. Histological analysis

Anesthetized mice were sacrificed and perfused with cold PBS. Subsequently, the hearts were carefully excised from the mice, fixed in phosphate-buffered 4 % formaldehyde solution for 24 h. After fixation, the hearts were embedded in either paraffin wax or optimal cutting temperature compound (OCT) for further processing. For paraffin-embedded heart tissues, sections with a thickness of 6 μm, while OCT-embedded heart tissues were sectioned at a thickness of 8 μm. For immunofluorescence staining, cryo-sections were permeabilized with 0.2 % Triton X-100, followed by incubation with a blocking buffer containing 1 % goat serum for 1 h at room temperature. Primary antibodies were then applied to incubate overnight at 4 °C. Subsequently, the sections were incubated with secondary antibodies for 1 h at room temperature. To visualize cell nuclei, the sections were stained with Hoechst 33342 (#H3570, Thermo Fisher Scientific, USA) for 10 min at room temperature. Finally, the sections were mounted using Fluoromount™ Aqueous Mounting Medium (#F4680, Sigma-Aldrich (Shanghai) Trading Co. Ltd). Immunofluorescence images were acquired using a Leica fluorescent microscope (model DM6000B, Leica, Germany).

2.8. Tissue collection and blood samples analysis

Mice were sacrificed at the indicated times and hearts were either snap-frozen in liquid nitrogen or fixed with 4 % paraformaldehyde (PFA) for further analysis. Mouse plasma samples were collected to measure total lactate dehydrogenase (LDH) using biochemistry analyzer (COBAS 8000, Roche, Switzerland) according to the manufacturer's instructions.

2.9. Liquid chromatography tandem mass spectrometry (LC-MS/MS) analysis of lipidomics

The mouse blood samples were collected into sodium citrate treated anticoagulant tubes at room temperature (RT) and centrifugation at 1000×*g* for 15 min. Then the plasma was obtained for LC-MS/MS analysis of lipidomics. The lipidomics was analyzed in Shanghai Applied Protein Technology Co., Ltd.

2.10. Measurement of infarct area and area at risk

Following a 24-h reperfusion period, the left anterior descending coronary artery in mice was occluded utilizing the identical suture positioned at the ligation site. To visualize the ischemic area at risk (AAR), a 1 % solution of evans blue dye was administered via the aorta. Subsequently, the heart was excised and thoroughly rinsed with phosphate-buffered saline (PBS). The ventricles were then subjected to freezing conditions at −20 °C for 30 min, followed by cross-sectioning the ventricles at 1 mm thickness. These cross-sectional segments were then submerged within a solution consisting of 1 % 2,3,5-triphenyltetrazolium chloride (TTC) diluted in PBS, allowing for a 15-min incubation period at a temperature of 37 °C to facilitate optimal staining. To halt the enzymatic reaction, 4 % paraformaldehyde (PFA) was promptly introduced. Utilizing the ImageJ 2.0 (NIH, USA), the infarct area (pale), AAR (red), as well as the total left ventricular (LV) area in both sides of each section were meticulously quantified. The resultant measurements were averaged to obtain representative values. The ratios of AAR to LV and infarct area to AAR were expressed as percentages.

2.11. Cardiomyocyte apoptosis analysis

Heart cryo-sections were subjected to processing using the *In Situ* Cell Death Detection Kit, TMR red (#12156792910, Roche, Germany). Subsequently, the cryo-sections were permeabilized with 0.2 % Triton X-100, followed by incubation with a blocking buffer containing 1 % goat serum for 1 h at RT and were then applied with αSA (#ab68167, Abcam, UK) overnight at 4 °C. Then, the sections were incubated with secondary antibodies for 1 h and stained with Hoechst for 10 min at RT. Finally, the sections were mounted with the Fluoromount™ Aqueous Mounting Medium. Immunofluorescence images were acquired using a Leica fluorescent microscope (model DM6000B, Leica, Germany).

2.12. Cardiomyocyte necrosis analysis

The heart cryo-sections were permeabilized with 0.2 % Triton X-100, followed by incubation with a blocking buffer containing 1 % goat serum for 1 h at RT. Then the sections were applied with αSA (#ab68167, Abcam, UK) and phosphor-MLKL (S345) (#ab196436,

Abcam, UK) overnight at 4 °C. Subsequently, the sections were incubated with secondary antibodies for 1 h and stained with Hoechst for 10 min at RT. Finally, the sections were mounted with the Fluoromount™ Aqueous Mounting Medium. Immunofluorescence images were acquired using a Leica fluorescent microscope (model DM6000B, Leica, Germany).

2.13. Isolation of mouse heart endothelial cells

Mice were sacrificed and hearts were transferred to ice-cold Dulbecco's modified Eagle's medium (DMEM), then digested in 1 mg/ml pre-warmed collagenase I (1 mg/mL, #C6885, Sigma Aldrich, Shanghai Trading Co. Ltd) and 60 units/ml DNase I (#10104159001, Roche Diagnostics Deutschland GmbH) at 37 °C for 45 min with gentle agitation. Following the digestion process, the resulting tissue suspension was passed through a 70-μm cell strainer to acquire a single cell suspension. After centrifugation, the cell pellets were resuspended in a solution containing 1 % fetal bovine serum (FBS) and 1 mM EDTA in phosphate-buffered saline (PBS). Subsequently, the single cell suspension was incubated with Biotin Rat Anti-Mouse CD31 antibody (#553370, BD Pharmingen, USA) conjugated to DynabeadsTM (#11035, Invitrogen, USA) for 30 min at RT with rotation. The Dynabeads were appropriately prepared according to the manufacturer's instructions. Following the separation step, the cells were thoroughly washed three times with the buffer to remove any unbound or non-specifically bound components. The cells were subsequently collected for further experimental procedures. The purity of isolated heart endothelial cells was 98.58 % ± 0.13 % (mean ± SD), as shown in the representative images of flow cytometric analysis by staining with the APC CD31 antibody (#561814, BD Pharmingen, USA) (Supplementary Fig. 1j).

2.14. The assessment of cardiomyocytes necrosis in vitro

To obtain mouse primary neonatal cardiomyocytes, neonatal mice at the age of postnatal 3 days were performed. The hearts of the mice were separated and cut into small pieces, and subsequently dissociated in Gibco's calcium-free HBSS, supplemented with 0.125 mg/mL trypsin, 0.1 mg/mL collagenase type IV (#C4-BIOC, Sigma, USA), and 10 mg/mL DNase I (#11284932001, Sigma, USA). The digestion process was conducted at 37 °C with constant stirring. Every 5 min, the supernatant was collected into a tube containing HBSS with 10 % FBS to halt the digestion process. This procedure was repeated approximately 8–10 times until the tissues were fully digested. The final collected supernatants were then centrifuged at 1000 rpm for 10 min and the resulting pellet was resuspended in DMEM enriched with 10 % FBS and 100 mM 5-bromo-20-deoxyuridine (#B5002, Sigma, USA). The suspension was strained through a 100 μm cell strainer, and the cells were seeded onto 10 cm plastic dishes and incubated for 2 h at 37 °C to deplete fibroblasts. Afterward, the cells were transferred to 1 % gelatin-coated dishes at a suitable density. The cells were cultured before experimental use.

The primary heart endothelial cell isolation was described as before [21]. Primary heart endothelial cells were cultured with Endothelial cell medium (ECM, #1001, ScienCell, USA) supplemented with 1 % endothelial cell growth factor (ECGS, #1052, ScienCell, USA) and 10 % FBS. Cardiomyocytes were cultured with DMEM enriched with 10 % FBS.

The experiment involving primary heart endothelial cells and cardiomyocytes was conducted in two steps. In the first step, primary heart endothelial cells, after being transfected with or without *scramble*, *S1pr2 shRNA* plasmids, *control* or *S1pr2* overexpression plasmids were subjected to a hypoxia/reoxygenation (H/R) injury model. After this treatment, supernatants from the primary heart endothelial cells were collected for further analysis. In the second step, primary cardiomyocytes were transfected with or without *scramble*, *S1pr2 shRNA* plasmids, *Control* or *S1pr2* overexpression plasmids, and subsequently treated with the collected supernatants. These cardiomyocytes were then also subjected to the H/R injury model. Following this, the cells were stained with propidium iodide (PI, 500 nM, #ST511, Beyotime, China) for 30 min at room temperature to assess cell necrosis. At last, the cells were fixed using a 4 % paraformaldehyde (PFA) solution for 15 min. Following fixation, the cells were washed and permeabilized with 0.1 % Triton X-100 PBS for 10 min. The cells were blocked in 1 % goat serum PBS solution for 1 h and incubated with αSA antibodies (#ab68167, Abcam, UK) overnight at 4 °C, and then secondary antibodies for 1 h at RT. Then, the cells were incubated with Hoechst to stain cell nuclei for 10 min at RT and mounted with Fluoromount™ Aqueous Mounting Medium (#F4680, Sigma-Aldrich, USA). Immunofluorescent images were captured by a Leica SP8 confocal laser scanning microscope (Leica, USA). Analysis of fluorescence images were performed with LAS X (Leica, USA) and ImageJ 2.0 (NIH, USA).

2.15. RNA-sequencing analysis

The heart tissues or primary heart endothelial cells were obtained as previously described. Isolated RNA was subsequently used for RNA-sequencing analysis. cDNA library construction and sequencing were performed by the Beijing Genomics Institute using BGISEQ-500 platform. Sequences of the clean data were mapped to the mouse reference genome (version GRCm38). The differentially expressed genes (DEGs), heat map, and GO enrichment analysis were performed in BGI Dr. Tom network platform (https://biosys.bgi.com). The original RNA-sequencing data discussed in this study were submitted on a public database and can be accessed via the Gene Expression Omnibus (GEO) series accession number: GSE245987 and GSE245988.

2.16. Cell culture

Human embryonic kidney (HEK) 293T cells were purchased from American Type Culture Collection (#CRL-1573, ATCC, USA), and a mouse cardiac microvascular endothelial cell line (CMVECs) was also used *in vitro* experiments, as previously reported [18,22]. All cells were cultured in Dulbecco's modified Eagle's medium of high glucose (#10-013-CV, Corning, USA) supplemented with 10 % FBS and 1 % Penicillin-Streptomycin (P–S).

To establish the cell models of hypoxia/reoxygenation injury (H/R), CMVECs were seeded in 6-well plates and starved with DMEM containing 1 % FBS and 1 % P–S, then the plates were transferred to a 1 % O_2 hypoxic incubator (94 % N_2, 5 % CO_2) for 6 h to induce hypoxic conditions. Afterward, the cells were returned to the normal incubator for reoxygenation for 24 h. In some experiments, CsA (1 μM, #S2286, Selleck, USA), Y27632 (10 μM, #S6390, Selleck, USA) or MCC950 (10 μM, #PZ0280, CP-456773 sodium salt, Sigma-Aldrich, USA) were added during the reoxygenation period. The cells were harvested for further RT-qPCR, western-blotting, or immunofluorescent staining analysis after reoxygenation.

2.17. Rho-GTP pull down assay

CMVECs were transfected with either *S1pr2* overexpression or *control* plasmids for 48 h in 10-cm dishes. Subsequently, the treated cells were carefully harvested and processed in accordance with the guidelines provided by the manufacturer of the Active Rho Pull-Down and Detection Kit (#16116, Thermo Fisher Scientific, USA).

2.18. Cell immunofluorescent staining

Cells were cultured on sterile glass cover slips, placed within 24-well plates, and subsequently fixed using a phosphate-buffered 4 % paraformaldehyde (PFA) solution for 15 min. Following fixation, the cells were washed and permeabilized with 0.1 % Triton X-100 PBS for 10 min. The cells were blocked in 1 % goat serum PBS solution for 1 h and incubated with primary antibodies overnight at 4 °C, and then secondary antibodies for 1 h at room temperature (RT) (Supplementary

Table 4). Then, cover slips were incubated with Hoechst to stain cell nuclei for 10 min at RT and mounted with Fluoromount™ Aqueous Mounting Medium (#F4680, Sigma-Aldrich, USA). Immunofluorescent images were captured by a Leica SP8 confocal laser scanning microscope (Leica, USA). Analysis of fluorescence images were performed with LAS X (Leica, USA) and ImageJ 2.0 (NIH, USA).

2.19. Mitochondrial morphology analysis

Cells were fixed in 4 % PFA solution for 15 min and subsequently permeabilized with 0.1 % Triton X-100 in PBS for 10 min. To assess mitochondrial morphology, the cells were blocked in a 1 % goat serum solution in PBS for 1 h, followed by incubation with Tomm20 antibody (#ab186735, Abcam, UK) overnight at 4 °C. Subsequently, the secondary antibody was applied for 1 h at RT, followed by Hoechst 33342 staining, and finally, the samples were mounted using Fluoromount™ Aqueous Mounting Medium. Mitochondrial morphology in individual cells were captured by a Leica SP8 confocal laser scanning microscope (Leica, USA). To measure the mitochondrial length, the average mitochondrial branch length (μm) was assessed in an unbiased way using the Mitochondrial Network Analysis (MiNA, https://github.com/StuartLab/MiNA) ImageJ macro [23].

2.20. Mitochondrial DNA (mtDNA) analysis

For visualization and measurement of mtDNA, cells were fixed in 4 % PFA solution and subsequently permeabilized with 0.1 % Triton X-100 in PBS for 10 min. Then the cells were blocked in a 1 % goat serum solution in PBS for 1 h, followed by incubation with Tomm20 antibody (#ab186735, Abcam, UK) and anti-DNA antibody (#690014S, Progen, Germany) overnight at 4 °C. Subsequently, secondary antibodies were applied for 1 h at RT. Nuclei were counterstained with Hoechst 33342 and finally, the samples were mounted using Fluoromount™ Aqueous Mounting Medium. Images were acquired with a Leica SP8 confocal laser scanning microscope (Leica, USA). Images analysis was performed with LAS X (Leica, USA) and ImageJ 2.0 (NIH, USA).

2.21. The opening of Mitochondrial Permeability Transition Pore (mPTP) detection

The cellular processing was conducted following the protocols and instructions provided by the manufacturer of Mitochondrial Permeability Transition Pore (mPTP) Assay Kit (#C2009S, Beyotime, China). In brief, cells were treated with calcein acetoxymethyl ester (calcein AM) and $CoCl_2$ for 30 min at 37 °C. Subsequently, immunofluorescence images were acquired using a Leica SP8 confocal laser scanning microscope (Leica, USA). Fluorescence analysis of images was performed with LAS X (Leica, USA) and ImageJ 2.0 (NIH, USA).

2.22. JC-1 flow cytometric analysis

The cellular processing was conducted following the protocols and instructions provided by the manufacturer of the Enhanced Mitochondrial Membrane Potential Assay Kit with JC-1 (#C2003S, Beyotime, China). Subsequently, the fluorescence intensity of each sample was measured and quantified using a CytoFLEX flow cytometer (#A00-1-1102, Beckman Coulter Life Sciences, USA).

2.23. Reactive oxygen species (ROS) detection assay

Cells were treated with 2′,7′-Dichlorodihydrofluorescein diacetate (DCFH-DA, 10 μM Selleck, #S9687) at 37 °C for 30 min. Subsequently, cells were fixed in 4 % PFA solution and nuclei were counterstained with Hoechst 33342 and finally, the samples were mounted using Fluoromount™ Aqueous Mounting Medium. Immunofluorescence images were acquired using a Leica SP8 confocal laser scanning microscope (Leica, USA). Fluorescence analysis of images was performed with LAS X (Leica, USA) and ImageJ 2.0 (NIH, USA). Additionally, cells were seeded into 96-well plates at 10,000 cells/well and then subjected to a H/R cell model. The cells were treated with 2′,7′-Dichlorodihydrofluorescein diacetate (DCFH-DA, 10 μM Selleck, #S9687) at 37 °C for 30 min at various reoxygenation time points (0 h, 1 h, 2 h, 6 h, 12 h and 24 h). Subsequently, the fluorescence was measured using a SpectraMax M5 reader (Molecular Devices, USA).

2.24. Lentiviral gene expression system

Lentiviral plasmids were packaged in HEK293T cells using lentiviral and package vectors pCMV.DR8, pMD2.G. Following a 48-h incubation after-transfection, the viral supernatants were collected, subjected to centrifugation, filtered through 0.4-μm filters and concentrated using the Lentivirus Concentration Kit (#GM-040801, Genomeditech, Shanghai, China). These viral supernatants were then applied to CMVECs in the presence of 10 μg/ml polybrene (#TR-1003, Sigma-Aldrich (Shanghai) Trading Co. Ltd) for a duration of 6–8 h. Subsequently, 48 h after infection, puromycin (#ST551-50 mg, Beyotime, China) was added to the medium at the concentration of 1 μg/ml for one week to obtain a pooled, drug-resistant population of CMVECs. The efficiency of infection was detected with fluorescence microscopy, RT-qPCR, and western-blotting.

2.25. Plasmid construction

To achieve *S1pr2* overexpression, the full-length cDNA of mouse *S1pr2* was subcloned into the CMV-MCS-PGK-Puro vector provided by Genomeditech (Shanghai) Co.,LTD. For the *S1pr2* gene-knockdown assay, the mouse shRNA specific to *S1pr2* was cloned into a U6-MCS-CMV-Puro vector.

Absolute quantification of *S1pr1*, *S1pr2* and *S1pr3* expression in primary heart endothelial cells and cardiomyocytes.

To achieve the absolute quantification of *S1pr1*, *S1pr2* and *S1pr3* expression in primary heart endothelial cells and cardiomyocytes. We first developed three control gene standards by constructing three plasmids, each containing cDNA fragments of mouse *S1pr1*, *S1pr2* or *S1pr3* genes, respectively. In brief, mouse cDNA fragments of *S1pr1*, *S1pr2* or *S1pr3* were subcloned into pUC57 vector. The cDNA fragments of *S1pr1*, *S1pr2* or *S1pr3* were synthesized by their specific qPCR primers, respectively (Supplementary Table 3). Next, for all three control gene standards, a seven-point standard curve (plot of CT values/crossing points of different standard dilutions against log of amount of standard) is generated using a dilution series of 7 different concentrations of the plasmids (10^8, 10^7, 10^6, 10^5, 10^4, 10^3, 10^2 copies/μl), the copy number of standard DNA molecules can be calculated using the following formula: (X ng/μl DNA x 10^{-9}/[plasmid length in base pairs x 660]) x 6.022 x 10^{23} = Y copies/μl. Finally, total RNAs were extracted from primary heart endothelial cells or cardiomyocytes. Subsequently, cDNA synthesis was described as previously. RT-qPCR experiments were conducted using the same primers previously utilized for subcloning cDNA fragments of the mouse genes *S1pr1*, *S1pr2* or *S1pr3* (Supplementary Table 3). The, CT values of the *S1pr1*, *S1pr2* or *S1pr3* were compared with their specific standard curves to determine the amount in the samples. At last, the absolute copy number of *S1pr1*, *S1pr2* or *S1pr3* in 1 μg total RNA was calculated.

2.26. RNA extraction and RT-qPCR

For quantitative PCR (qPCR) analysis, total RNAs were extracted from heart tissues, heart endothelial cells (ECs), or cultured cell lines using the TRIzol reagent (#15596018, Invitrogen, USA). Subsequently, cDNA synthesis was carried out using the HiScript II Q RT SuperMix for qPCR (+gDNA wiper) kit (#R223-01, Vazyme Biotech, China) to reverse transcribe the RNA into complementary DNA (cDNA). RT-qPCR

experiments were performed with different primers (Supplementary Table 3) using the AceQ Universal SYBR qPCR Master Mix (#Q511-02, Vazyme Biotech, China) on a QuantStudio™6 Flex Real-time PCR system (Applied Biosystems, USA) according to the manufacturer's protocol. To ensure accurate normalization of the data, the values obtained for the housekeeping gene *β-actin* were employed as internal controls. Transcript quantities were normalized to *β-actin* (ACTB) expression using a widely used method of $2^{-\text{deltadeltaCT}}$ to present relative gene expression.

2.27. SDS-PAGE and western-blotting

Cells or tissues were carefully harvested and then lysed using a lysis buffer (#P0013C, Beyotime, China) supplemented with a protease inhibitor cocktail (#539131, Calbiochem, USA) and phenylmethylsulfonyl fluoride (PMSF, #ST505, Beyotime, China) on ice for 10 min. After 15 min of centrifugation at 4 °C, the supernatants were collected. The protein concentration in the lysates was quantified using the Bradford method and the BCA protein assay kit (#P0012S, Beyotime, China). Equal amounts of protein samples were subjected to separation via sodium dodecyl sulfate-polyacrylamide gel electrophoresis (SDS-PAGE) using gels with acrylamide concentrations of 10 %, 12.5 %, or 15 % (Shanghai Epizyme Biomedical Technology Co., Ltd), and then transferred onto a PVDF membrane (#IPVH00010, Millipore, USA). After blocking with 5 % non-fat milk in PBST, the membranes were incubated with primary antibodies (Supplementary Table 4), followed by the application of HRP-linked secondary antibodies.

2.28. Statistical analysis

Data were presented as mean ± standard error of mean (S.E.M.) for at least three independent assays unless otherwise noted. All data passed the normality and equal variance before analysis. Differences between 2 groups were examined using student *t*-test and comparisons between multiple groups examined by one-way or two-way ANOVA, followed by Tukey's multiple comparisons test. GraphPad Prism software (version 8.0) and SPSS 11.0 (SPSS. Inc) were employed to perform all statistical analyses, and values of $P < 0.05$ were considered statistically significant.

3. Results

3.1. The alteration of plasma S1P levels after cardiac I/R injury is involved in the process of I/R injury

We first applied LC-MS/MS to screen the lipidomic profile in plasma of mice following a cardiac I/R injury operation. We found multiple lipid molecules were down-regulated after heart I/R (Fig. 1a and Supplementary Figs. 1a–c). Notably, we detected sphingosine lipids, including sphingosine 1-phosphate (S1P), were significantly reduced in plasma after cardiac I/R injury (Fig. 1a–b), in an agreement with previous reports [24,25]. In consistence with our animal experiment, measurement of S1P in patients showed that plasma S1P levels were significantly reduced in coronary heart disease (CHD) patients after PCI, compared with those without PCI operation (Fig. 1c and Supplementary Table 1), suggesting that the altered S1P levels might be involved in the process of cardiac I/R injury. Previous reports showed that plasma S1P displayed a protective effect on heart injuries [26,27]. To investigate whether the elevated plasma S1P might protect the heart from I/R injury, we used THI or DOP, S1P lyase inhibitors, to block S1P degradation by antagonizing S1P lyase to increase S1P plasma levels *in vivo*. As expected, THI or DOP treatment evidently increased plasma S1P levels (Fig. 1d and Supplementary Fig. 1d) and significantly reduced the infarct size while the AAR/LV (the ischemic area at risk/left ventricular area) was not altered between THI or DOP and control group in cardiac I/R injury model (Fig. 1e and Supplementary Fig. 1e). As expected, serum levels of lactic dehydrogenase (LDH), a general indicator of cardiac injury, were significantly decreased in mice treated with THI or DOP compared with the control group (Fig. 1f and Supplementary Fig. 1f). These results indicate that the elevation of S1P levels ameliorates myocardial I/R injury.

As previous studies showed that S1P exerted its protective effects on hearts via S1PR1 signaling and our study confirmed that S1PR1 was mainly expressed in endothelial cells of cardiac tissues [17,21,28], we investigated whether S1P might influence cardiac I/R injuries via EC-S1PR1. We therefore generated EC-specific *S1pr1* knock-out mice ($S1pr1^{ECKO}$), as previously reported [20,21]. As expected, $S1pr1^{ECKO}$ mice exhibited larger cardiac infarct size than *WT* mice, although the ratio of AAR/LV was comparable between $S1pr1^{ECKO}$ and *WT* mice (Fig. 1g–h and Supplementary Figs. 1g–h). Consistently, serum LDH levels were significantly increased in $S1pr1^{ECKO}$ mice compared with *WT* mice (Fig. 1i and Supplementary Fig. 1i), indicating that S1P/S1PR1 signaling displays a protective effect on cardiac I/R injury. Surprisingly, $S1pr1^{ECKO}$ mice treated with THI or DOP displayed a larger infarct size and higher serum LDH levels than $S1pr1^{ECKO}$ mice with THI or DOP vehicle control, which contrasted with a smaller infarct size and lower levels of serum LDH in the *WT* mice treated with THI or DOP than *WT* mice treated with the control vehicle (Fig. 1d–i and Supplementary Figs. 1d–i), suggesting that in addition to the protective effect of EC-S1PR1 on cardiac I/R injury, other S1P receptor subtypes might exert a detrimental effect on hearts.

3.2. EC-specific loss of S1PR2 alleviates cardiac I/R injury and inflammatory responses

To clarify which subtype of S1P receptors other than S1PR1 might be involved in the process of cardiac I/R injury, we examined the expression profile of S1P receptors in hearts. As previously reported [29,30], three subtypes of S1P receptors, including S1PR1, S1PR2 and S1PR3, are expressed in cardiac tissues (Fig. 2a–b). Our data showed that the expression of *S1pr2* mRNA levels were significantly up-regulated in cardiac tissues after I/R, while neither *S1pr1* nor *S1pr3* mRNA levels altered in I/R hearts (Fig. 2b), suggesting that *S1pr2* might play an important role in cardiac I/R injury. The previous investigations from Christopher K. Means and colleagues revealed that both S1PR2 and S1PR3 mediated Akt activation in cardiomyocytes, which contributes to the protective effects of S1PR2 and S1PR3 on myocardial ischemia-reperfusion injury [31]. In consistence with this investigation, we also observed that CM-expressing S1PR2 protected cardiomyocytes from cell necrosis upon H/R injury *in vitro* (Supplementary Figs. 2a–b). Since we observed that *S1pr2* was expressed in cardiac endothelial cells as well (Supplementary Figs. 1j–k), we next investigated whether EC-expressing S1PR2 might affect cardiomyocyte necrosis through a paracrine mechanism. We therefore treated cardiomyocytes with EC-conditioned medium. The results demonstrated that the conditioned medium obtained from *S1pr2*-overexpressing ECs exacerbated H/R-induced cardiomyocyte necrosis, while the conditioned medium from *S1pr2*-silencing ECs ameliorated their cell necrosis (Supplementary Figs. 2c–d), suggesting that EC-S1PR2 exerted a detrimental effect on cardiomyocyte survival during H/R injury. We subsequently conducted experiments involving *S1pr2*-silencing CMs treated with the conditioned medium obtained from *S1pr2*-silencing ECs. Notably, no difference of cardiomyocyte necrosis was observed upon H/R (Supplementary Fig. 2e). Similarly, no difference of cardiomyocyte necrosis was detected in both *S1pr2*-overexpressing CMs treated with the conditioned medium from *S1pr2*-overexpressing ECs (Supplementary Fig. 2f). These results indicated that the divergent actions of S1PR2 in cardiomyocytes and endothelial cells during I/R injury might mask the specific cellular role of S1PR2, highlighting the cell-specific effects of *S1pr2* on I/R injury. We further observed that *S1pr2*/S1PR2 was significantly up-regulated in vascular endothelial cells (ECs) after cardiac I/R injury (Fig. 2c–d); however, neither S1PR1 nor S1PR3 was altered in ECs after I/R (Fig. 2c), we hypothesized that EC-expressing S1PR2 might play a cell-specific

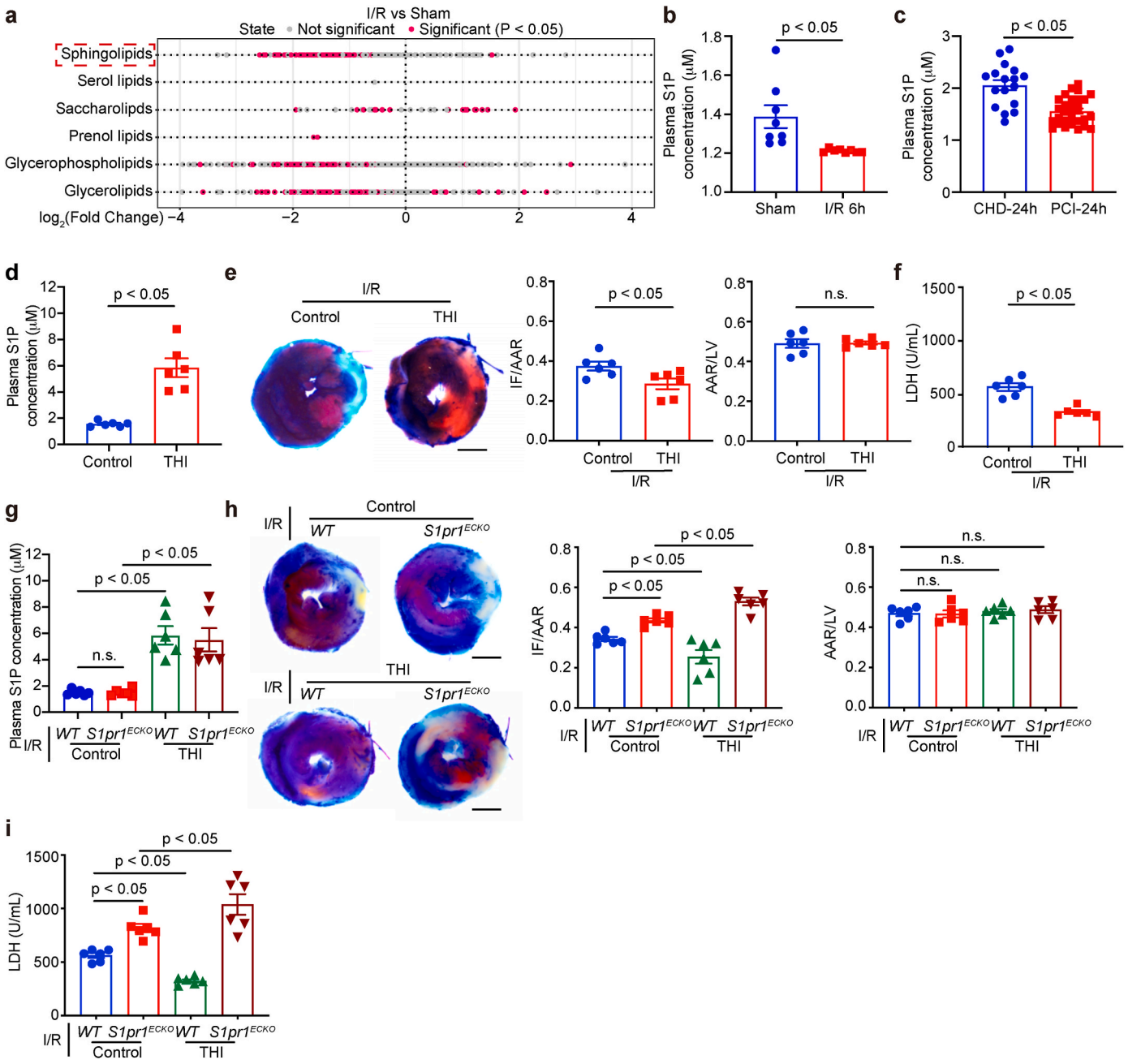

Fig. 1. S1P is involved in the process of heart ischemia/reperfusion injury. **a** Dot plot showed the individual lipids in the plasma of mice after cardiac ischemia-reperfusion (I/R) injury (45 min of ischemia/6 h of reperfusion) expressed as $\log_2$ (fold change) versus the plasma of the control mice after sham operations (n = 3 per group). The dashed red box highlights sphingosine lipids that are down-regulated after cardiac I/R. **b-c** Sphingosine 1-Phosphate (S1P) concentrations in the plasma of the mice after cardiac I/R injury (45 min of ischemia/6 h of reperfusion) compared to the mice after sham operations by ELISA (n = 8 per group) (**b**), and the S1P concentrations in the plasma of patients diagnosed with coronary heart disease (CHD) at 24 h after coronary angiography procedures (CAG-24h, n = 17 per group) or percutaneous coronary intervention (PCI-24h, n = 28 per group) by ELISA (**c**). **d** The plasma S1P concentration in the mice after S1P lyase inhibitor 2-Acetyl-5-tetrahydroxybutyl Imidazole (THI) treatment compared to control mice by ELISA (n = 6 per group). **e** Representative images of evans blue/triphenyl-2H-tetrazolium chloride (TTC) staining of heart tissue sections collected from mice treated with PBS or THI after I/R injury (45 min of ischemia/24 h of reperfusion), with their quantification of the infarct area (IF), at-risk area (AAR), and left ventricle (LV) (n = 6 per group). **f** Serum LDH (lactate dehydrogenase) levels of mice treated with PBS or THI after cardiac I/R injury (45 min of ischemia/24 h of reperfusion) were measured (n = 6 per group). **g** The plasma S1P concentration of mice in the indicated groups by ELISA (n = 6 per group). **h** Representative images of evans blue/TTC-staining of heart tissue sections collected from *WT* or *S1pr1*^{ECKO} mice treated with PBS or THI after cardiac I/R injury (45 min of ischemia/24 h of reperfusion), with their quantification of the infarct area (IF), at-risk area (AAR), and left ventricle (LV) area (n = 5–6 per group). **i** Serum LDH levels of *WT* or *S1pr1*^{ECKO} mice treated with PBS or THI after cardiac I/R injury (45 min of ischemia/24 h of reperfusion) were measured (n = 6 per group). Data were shown as mean ± SEM. n.s. indicated not significant. Scale bars: **e** and **h**, 2 mm. Unpaired Student's t-test (**b**, **c**, **d**, **e** and **f**). One-way ANOVA (**g**, **h** and **i**).

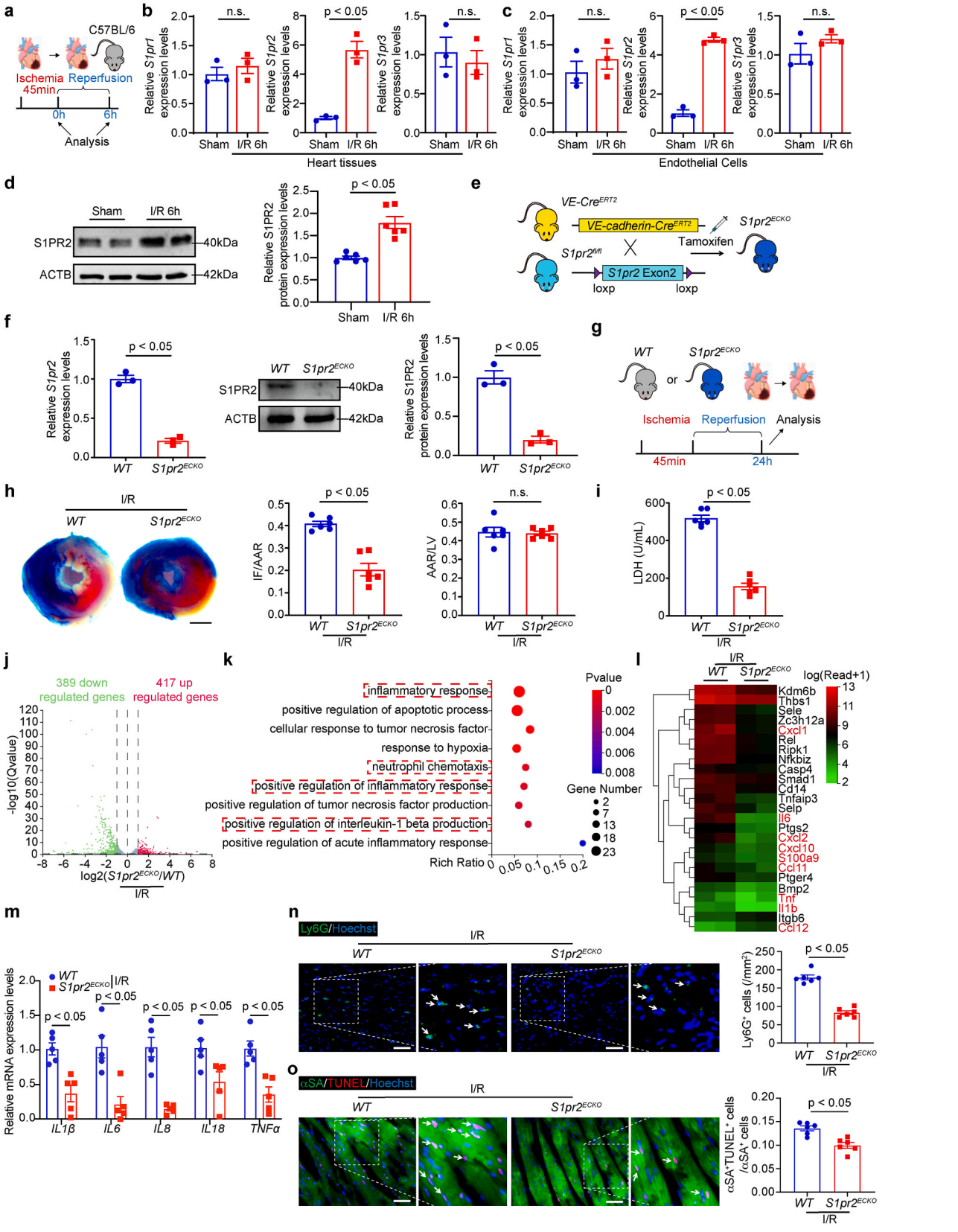

(caption on next page)

Fig. 2. The EC-specific loss of S1PR2 alleviates cardiac I/R injury and inflammatory responses. **a** Schematic diagram showed the mouse model of cardiac I/R injury. **b-d** Relative mRNA expression levels of *S1pr1, S1pr2* and *S1pr3* in heart tissues of mice after cardiac I/R injury (45 min of ischemia/6 h of reperfusion) compared to those of sham control mice by RT-qPCR (**b**), relative mRNA expression levels of *S1pr1, S1pr2* and *S1pr3* in cardiac endothelial cells (ECs) after cardiac I/R injury (45 min of ischemia/6 h of reperfusion) compared with those of sham control mice by RT-qPCR (**c**) (n = 3), and western-blotting analysis of S1PR2 protein expression levels in cardiac endothelial cells (ECs) after cardiac I/R injury (45 min of ischemia/6 h of reperfusion) compared with those of sham control mice (**d**) (n = 3). **e-f** Schematic diagram showed the generation of EC-specific *S1pr2* loss-of-function mice (**e**), relative mRNA expression levels of *S1pr2* in heart ECs of *WT* and $S1pr2^{ECKO}$ mice by RT-qPCR and relative S1PR2 protein expression levels by western-blotting (n = 3 per group) (**f**). **g** Schematic diagram showed the mouse model of cardiac I/R injury. **h** The representative images of evans blue/TTC-staining of heart tissue sections collected from *WT* or $S1pr2^{ECKO}$ mice after cardiac I/R injury (45 min of ischemia/24 h of reperfusion), with their quantification of the infarct area (IF), at-risk area (AAR), and left ventricle (LV) (n = 6 per group). **i** Serum LDH levels of *WT* or $S1pr2^{ECKO}$ mice after cardiac I/R injury 45 min of ischemia/24 h of reperfusion) were measured (n = 6 per group). **j** A volcano plot illustrated different gene expression from RNA-sequencing analysis in heart tissues between the *WT* control mice after cardiac I/R injury and $S1pr2^{ECKO}$ mice after cardiac I/R injury. 389 downregulated genes (green) and 417 upregulated genes (red) were shown (n = 2). **k-l** Gene ontology (GO) enrichment analysis (**k**) and the heat map (**l**) of differentially expressed genes in heart tissues between $S1pr2^{ECKO}$ mice after cardiac I/R injury compared and the *WT* control after cardiac I/R injury (n = 2). The dashed red boxes highlight inflammatory response, positive regulation of inflammatory response and positive regulation of interleukin-1 beta production that are enriched in GO analysis. **m** Relative mRNA expression levels of *IL1β*, *IL6*, *IL8*, *IL18* and *TNFα* in heart tissues of $S1pr2^{ECKO}$ mice compared to *WT* mice after cardiac I/R injury (45 min of ischemia/24 h of reperfusion) by RT-qPCR (n = 5 per group). **n-o** The representative images of immunofluorescence-staining of Ly6G (**n**) and cardiomyocytes apoptosis by co-immunofluorescence-staining of αSA and TUNEL (**o**) in $S1pr2^{ECKO}$ mice compared to *WT* mice after cardiac I/R injury (45 min of ischemia/24 h of reperfusion) (n = 6 per group). Data were shown as mean ± SEM. n.s. indicated not significant. Scale bars: **h**, 2 mm. **n**, **o**, 50 μm. Unpaired Student's t-test (**b**, **c**, **d**, **f**, **h**, **i**, **m**, **n** and **o**).

role for cardiac I/R injury.

To examine the effect of EC-S1PR2 on cardiac I/R injury *in vivo,* we generated EC-specific *S1pr2* knock-out mice ($S1pr2^{ECKO}$) by breeding *the VE-cadherin-Cre*^{ERT2} line with $S1pr2^{flox/flox}$ mice (Fig. 2e). A significant reduction in *S1pr2* mRNA and S1PR2 protein levels was observed in ECs obtained from $S1pr2^{ECKO}$ mice after tamoxifen treatment, as shown by RT-qPCR and western-blotting (Fig. 2f). In cardiac I/R model (Fig. 2g), $S1pr2^{ECKO}$ mice exhibited a similar ratio of AAR/LV as *WT* mice; however, the cardiac infarct size was significantly decreased in $S1pr2^{ECKO}$ mice compared with *WT* littermates (Fig. 2h). Meanwhile, lower levels of serum LDH were observed in $S1pr2^{ECKO}$ mice than *WT* mice (Fig. 2i). Our data showed that the EC-specific loss of S1PR2 led to an improvement in cardiac I/R injury, suggesting that EC-expressing S1PR2 exerted a detrimental effect on cardiac I/R injury.

To further reveal the pathological mechanism by which EC-S1PR2 influences cardiac I/R injury, we performed RNA sequencing of cardiac tissues after I/R in $S1pr2^{ECKO}$ mice and *WT* mice. Our results showed 806 unique differentially expressed genes (DEGs) in $S1pr2^{ECKO}$ hearts after cardiac I/R (Fig. 2j). Gene Ontology (GO) enrichment analysis showed that downregulated genes in $S1pr2^{ECKO}$ mice after cardiac I/R injury were associated with inflammatory responses and multiple inflammatory-related biological processes compared with *WT* littermates after cardiac I/R injury (Fig. 2k-l), indicating that S1PR2 deficiency in ECs reduced inflammatory responses after cardiac I/R. Further quantitative RT-qPCR analysis showed a significant decrease of multiple inflammatory factors, including *IL1β*, *IL6*, *IL8*, *IL18* and *TNFα*, in post-I/R hearts (Fig. 2m). Neutrophils accumulation in cardiac tissue contributed to the elevated inflammatory response in I/R hearts. We thus performed immunostaining of Ly6G, a neutrophil marker, to examine neutrophil infiltration in post-I/R hearts, and our data showed significantly less neutrophils infiltration in cardiac tissues in $S1pr2^{ECKO}$ mice compared with *WT* littermates (Fig. 2n). As expected, TUNEL staining showed that $S1pr2^{ECKO}$ mice significantly reduced cardiomyocyte apoptosis after I/R injury, in comparison with *WT* control mice (Fig. 2o). Additionally, $S1pr2^{ECKO}$ showed less cardiomyocytes necrosis after cardiac I/R injury (Supplementary Fig. 3a). These results supported that EC-specific loss of S1PR2 diminished I/R-induced cardiac inflammation and cardiomyocyte apoptosis, contributing to the protective effect on cardiac I/R injury.

3.3. The EC-specific S1PR2 overexpression aggravates cardiac I/R injury

To further confirm the effect of EC-S1PR2 on cardiac I/R injury *in vivo*, we generated EC-specific *S1pr2* gain-of-function mice ($S1pr2^{ECTg}$) by crossing the *VE-cadherin-CreERT2* line with $S1pr2^{Tg/WT}$ mice (Supplementary Fig. 4a). The expression levels of *S1pr2*/S1PR2 were significantly elevated in ECs of $S1pr2^{ECTg}$ mice after tamoxifen treatment, as shown by RT-qPCR and western-blotting (Supplementary Fig. 4a). Our *in vivo* data showed that the cardiac infarct size of $S1pr2^{ECTg}$ mice was larger than *WT* littermates, without alteration in the ratio of AAR/LV (Supplementary Fig. 4b). As expected, serum LDH levels significantly increased in $S1pr2^{ECTg}$ mice after cardiac I/R injury compared with *WT* mice (Supplementary Fig. 4c). We next observed higher levels of multiple inflammatory factors, including *IL1β*, *IL6*, *IL8*, *IL18* and *TNFα* in post-I/R hearts of $S1pr2^{ECTg}$ mice than *WT* mice (Supplementary Fig. 4d), which was consistent with our observation that $S1pr2^{ECTg}$ mice exhibited more neutrophil infiltration in post-I/R myocardium (Supplementary Fig. 4e). Consequently, the EC-specific S1PR2 overexpression aggravated cardiomyocyte apoptosis and necrosis after I/R injury, in comparison with *WT* control mice (Supplementary Figs. 4f–g). Together with our results obtained from $S1pr2^{ECKO}$ mice, these data from $S1pr2^{ECTg}$ mice confirmed a crucial role of EC-S1PR2 for cardiac I/R injury.

3.4. EC-S1PR2 triggers NLRP3 inflammasome activation and subsequently induces endothelial pyroptosis

To further disclose the detailed mechanism underlying the effect of EC-S1PR2 on cardiac I/R injury, we isolated primary cardiac ECs from $S1pr2^{ECKO}$ and *WT* mice after cardiac I/R injury, and performed RNA sequencing of these cells. RNA sequencing data showed that the loss of S1PR2 in endothelial cells resulted in 905 DEGs after cardiac I/R (Fig. 3a). GO enrichment analysis showed that downregulated genes were related to inflammatory responses, NLRP3 inflammasome activation and pyroptosis after cardiac I/R (Fig. 3b–c and Supplementary Fig. 5a), indicating the key role of S1PR2 for inflammasome activation and pyroptosis in ECs after cardiac I/R. We next treated CMVECs with hypoxia for 6 h following with reoxygenation for 24 h *in vitro* to simulate I/R injury. Our western-blotting analysis showed that *S1pr2* knockdown reduced the levels of multiple inflammasome factors, including NLRP3, active IL1β, and cleaved CASPASE1 upon hypoxia/reoxygenation (H/R) condition, whereas *S1pr2* overexpression increased the levels of the above inflammasome factors, confirming that S1PR2 plays an essential role in the regulation of EC inflammasome activation (Fig. 3d–f and Supplementary Figs. 5b–f).

It has been shown that inflammasome activation triggered pyroptosis, a distinct form of inflammatory cell death via the proteolytic cleavage of gasdermin D (GSDMD) by CASPASE1 [32,33]. We next asked whether S1PR2 was involved in EC pyroptosis via inflammasome activation. Our western-blotting analysis showed that *S1pr2* overexpression increased the levels of cleaved GSDMD (Fig. 3e and Supplementary Fig. 5e), while *S1pr2* knockdown reduced GSDMD cleavage (Fig. 3f and Supplementary Fig. 5f). Immunostaining of cleaved GSDMD in ECs further supported that *S1pr2* overexpression enhanced cell

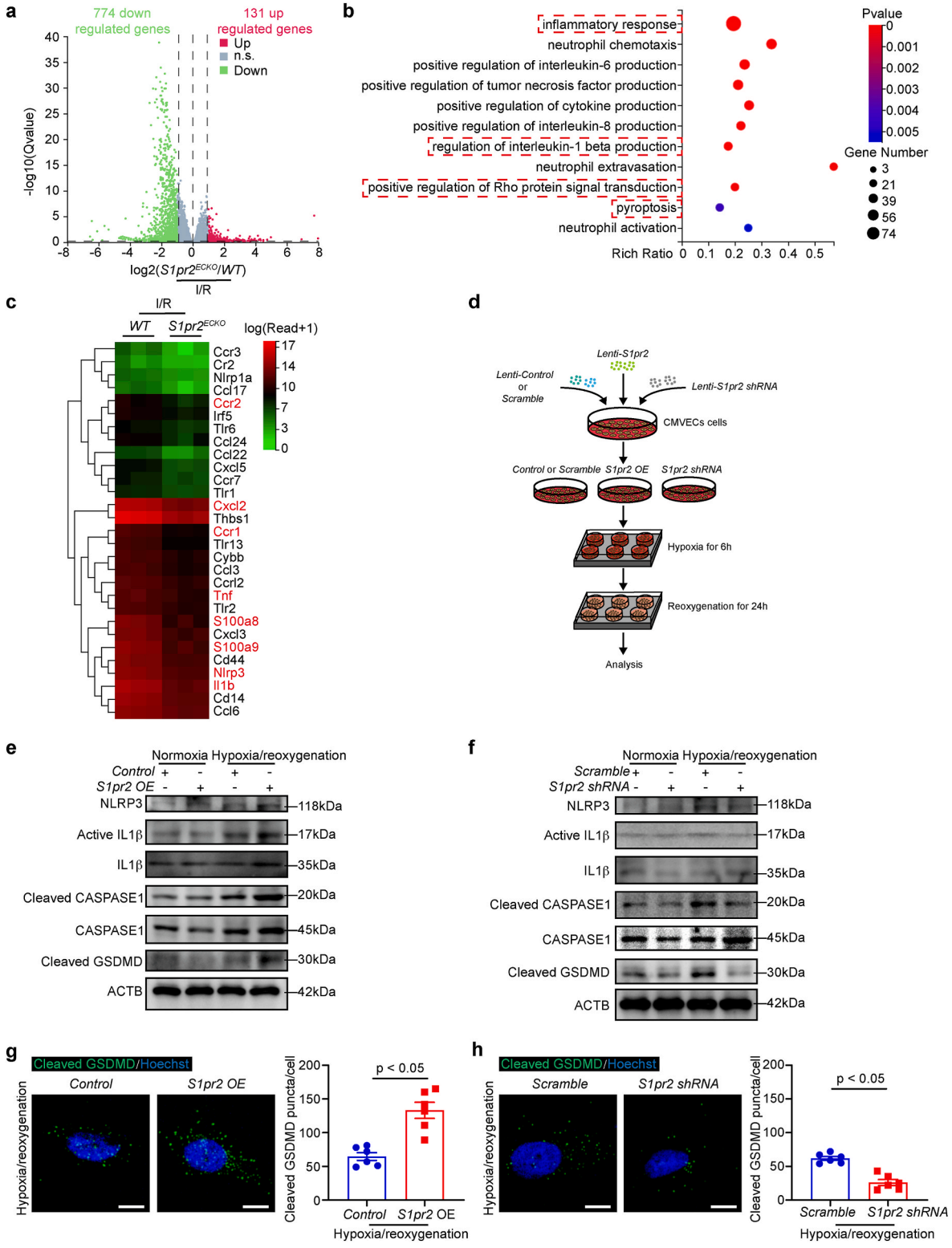

Fig. 3. EC-S1PR2 triggers NLRP3 inflammasome activation and subsequently induces endothelial pyroptosis. **a** A volcano plot illustrated different gene expression from RNA-sequencing analysis in cardiac endothelial cells from the *WT* control mice after cardiac I/R injury and *S1pr2*^{ECKO} mice after cardiac I/R injury. 774 downregulated genes (green) and 131 upregulated genes (red) were shown (n = 3). **b-c** Gene ontology (GO) enrichment analysis (**b**) and the heat map of differentially expressed genes (**c**) in cardiac endothelial cells from *S1pr2*^{ECKO} mice after cardiac I/R injury compared with *WT* control after cardiac I/R injury (n = 3). The dashed red boxes highlight inflammatory response, regulation of interleukin-1 beta production, positive regulation of Rho protein signal transduction and pyroptosis that are enriched in GO analysis. **d** Schematic diagram showed the *in vitro* experimental model of hypoxia reoxygenation (H/R, 6 h of hypoxia/24 h of reoxygenation) injury. **e-f** Western-blotting analysis of NLRP3, active IL1β, cleaved CASPASE1 and cleaved GSDMD protein expression levels in the indicated groups (n = 3 per group). **g-h** Representative images of pyroptosis in CMVECs of the indicated groups (H/R, 6 h of hypoxia/24 h of reoxygenation) by immunofluorescence-staining of cleaved GSDMD (n = 6 per group). Data were shown as mean ± SEM. Scale bars: **g**, **h**, 10 μm. Unpaired Student's t-test (**g** and **h**).

pyroptosis, whereas *S1pr2* knockdown inhibited cell pyroptosis (Fig. 3g–h). We next examined whether the effect of S1PR2 on EC pyroptosis was dependent on NLRP3 inflammasome activation. We took advantage of NLRP3 inhibitor, MCC950, to block NLRP3 inflammasome activation. Our data showed that MCC950 reversed the enhancing effect of *S1pr2* overexpression on NLRP3 inflammasome activation and inhibited EC pyroptosis aggravated by *S1pr2* overexpression (Supplementary Fig. 5g-l). These data suggest that EC-S1PR2 plays an essential role in the process of EC pyroptosis via triggering NLRP3 inflammasome activation.

3.5. EC-S1PR2 induces excessive mitochondrial fission upon hypoxia/reoxygenation injury

It has been shown that mitochondria disorder contributed to inflammasome activation and cell pyroptosis [34,35], further influencing cardiac I/R injury [36]. We thus examined whether EC-S1PR2 affected mitochondria disorder upon hypoxia/reoxygenation injury. Mitochondrial permeability transition pore (mPTP) assay showed that *S1pr2* overexpression increased mitochondrial membrane permeability, while *S1pr2* knockdown protected EC mitochondrial membrane integrity from hypoxia/reoxygenation injury (Fig. 4a–b). Treatment of Cyclosporin A (CsA, 1 μM), an inhibitor of mPTP opening [37,38], eliminated the effect of *S1pr2* overexpression on mPTP (Fig. 4a–b). Due to damaged membrane integrity, the mitochondrial membrane potential depolarization was increased in *S1pr2*-overexpressing ECs after hypoxia/reoxygenation, as shown by cytometric analysis of JC-1 (Supplementary Fig. 6a). Moreover, *S1pr2* overexpression increased intracellular reactive oxygen species (ROS) production by 2′, 7′-Dichlorodihydrofluorescein diacetate (DCFH-DA) staining and assay (Supplementary Figs. 6c and 6e). In contrast to *S1pr2* overexpression, *S1pr2*-knockdown exhibited a higher mitochondrial potential (Supplementary Fig. 6b) and less intracellular ROS production (Supplementary Figs. 6d and 6f). We next examined mitochondrial morphology by Tomm20 staining. Our data showed that *S1pr2* overexpression resulted in higher extent of mitochondrial fission, leading to the formation of fragmented mitochondria with shorter lengths, in comparison with the control group, under hypoxia/reoxygenation conditions (Fig. 4c). Conversely, *S1pr2* down-regulation suppressed mitochondrial fission, thus normalizing the mitochondrial morphology in hypoxia/reoxygenation-treated ECs (Fig. 4d). It has been shown that mitochondrial hyperfission and increased fragmentation resulted in mitochondrial damage and mtDNA release into cytoplasm [39,40]. As expected, we observed a significant increase of cytoplasmic mtDNA in *S1pr2*-overexpressing ECs upon hypoxia/reoxygenation injury, while *S1pr2* knockdown inhibited mtDNA release into EC cytoplasm (Fig. 4e–f). Overall, EC-S1PR2 overexpression aggravated I/R-induced mitochondria damage, which was characterized by disordered mitochondrial dynamics, a reduced mitochondrial membrane potential and increased mtDNA release; however, EC-S1PR2 knockdown attenuated these pathological alterations in EC mitochondria.

3.6. EC-S1PR2 activates RHO/ROCK1/DRP1 to induce mitochondrial hyperfission, leading to mtDNA release into cytoplasm which triggers NLRP3 inflammasome activation, and subsequently induces endothelial pyroptosis

It has been shown that S1PR2 regulated RHO signaling pathway [41,42]. Pull-down assay showed that S1PR2 increased the levels of RHO-GTP (Fig. 5a). As RHO signaling regulates phosphorylation of ROCK1 [43], we further examined whether S1PR2 influenced the active status of ROCK1. Our western-blotting analysis showed that *S1pr2* overexpression significantly enhanced the active status of ROCK1, while *S1pr2* knockdown reduced ROCK1 activation, as indicated by the ratio of phosphorylation levels of ROCK1 to total ROCK1 levels (Fig. 5b–c and Supplementary Figs. 7a–b). Recent studies revealed that ROCK1 signaling affected DRP1 activation [44,45]. We thus investigated whether EC-S1PR2 regulated the activity of DRP1 via ROCK1 signaling pathway. Our data showed that S1PR2 knockdown reduced the phosphorylation of DRP1, whereas S1PR2 overexpression enhanced the active levels of DRP1 (Fig. 5b–c and Supplementary Figs. 7a–b). The enhancing DRP1 activity upon S1PR2 overexpression was further blocked by ROCK1 inhibitor, Y27632, indicating that the regulation of S1PR2 on DRP1 activity was dependent on ROCK1 signaling pathway (Fig. 5c–d and Supplementary Fig. 7c). It has been shown that ROCK1/DRP1 signaling pathway was essential for the regulation of mitochondrial fission and homeostasis [44,45]. We further examined whether S1PR2 controlled mitochondria functions and homeostasis via ROCK1/DRP1 signaling pathway. Our results showed that ROCK inhibitor reversed the increased mitochondrial membrane permeability, mitochondrial membrane potential depolarization and intracellular ROS production (Fig. 5e and Supplementary Figs. 7e–g). Further Tomm20 staining showed that Y27632 inhibited the excessive mitochondrial fission and fragmentation triggered by S1PR2 overexpression in ECs (Fig. 5f). Consistently, the inhibition of ROCK1 signaling pathway reduced mtDNA leakage triggered by S1PR2 overexpression (Fig. 5g). These results suggest that EC-S1PR2 regulates mitochondrial fission via ROCK1/DRP1 signaling pathway. We next examined whether the effect of EC-S1PR2 on inflammasome activation and cell pyroptosis were dependent on ROCK1 signaling pathway. As expected, the inhibition of ROCK signaling reversed the enhancing effect of S1PR2 overexpression on inflammasome activation and cell pyroptosis (Fig. 5h–i and Supplementary Fig. 7d). Collectively, our data support that S1PR2 activates RHO/ROCK1/DRP1 signaling pathway, which leads to the mitochondria hyperfission and thus results in mtDNA leakage into cytoplasm, triggering inflammasome activation and subsequently inducing cell pyroptosis in ECs.

3.7. EC-S1PR2 overexpression aggravates cardiac I/R injury via NLRP3 inflammasome activation

To further confirm whether NLRP3 inflammasome activation was involved in the effect of EC-S1PR2 overexpression on cardiac I/R injury *in vivo*, we generated EC-specific *Nlrp3* knock-out mice ($Nlrp3^{ECKO}$) with $S1pr2^{ECTg}$ mice. The expression levels of *Nlrp3*/NLRP3 were significantly reduced in ECs of $Nlrp3^{ECKO}$ mice, as shown by RT-qPCR and western-blotting (Supplementary Figs. 8a–b). Our *in vivo* studies showed that EC-specific *Nlrp3* deletion reversed the enhancing effect of EC-S1PR2 overexpression on cardiac infarct size in I/R injury model (Fig. 6a). The serum LDH levels were significantly reduced in $Nlrp3^{ECKO}$;$S1pr2^{ECTg}$ mice after cardiac I/R injury, in comparison with $S1pr2^{ECTg}$ mice (Fig. 6b). As expected, EC-specific *Nlrp3* deletion evidently reduced the levels of inflammatory factors, including *IL1β*, *IL6*, *IL8*, *IL18* and *TNFα* (Fig. 6c), which should be significantly elevated in post-I/R hearts of $S1pr2^{ECTg}$ mice (Supplementary Fig. 4d). Our further histological studies showed that EC-NLRP3 knock-out abolished the enhancing effects of EC-S1PR2 overexpression on neutrophil infiltration (Fig. 6d). As expected, the reduced apoptotic and necrotic cardiomyocytes were observed in $Nlrp3^{ECKO}$;$S1pr2^{ECTg}$ mice after cardiac I/R injury (Fig. 6e and Supplementary Fig. 8c). Together with our *in vitro* results, these *in vivo* data confirmed that EC-S1PR2 regulated NLRP3 inflammasome activation, which contributed to the detrimental effect of EC-S1PR2 overexpression on inflammatory responses and cardiac I/R injury.

3.8. EC-specific GSDMD knockdown abolishes the detrimental effects of EC-S1PR2 overexpression on cardiac I/R injury in vivo

To further confirm the GSDMD-triggered cell pyroptosis was involved in the effect of EC-S1PR2 overexpression on cardiac I/R injury *in vivo*, we applied AAV9 to express *Gsdmd* shRNA under the EC-specific promoter, *Tie2*, in $S1pr2^{ECTg}$ mice. RT-qPCR and western-blotting analysis showed that *AAV9-Tie2-Gsdmd shRNA* significantly reduced the

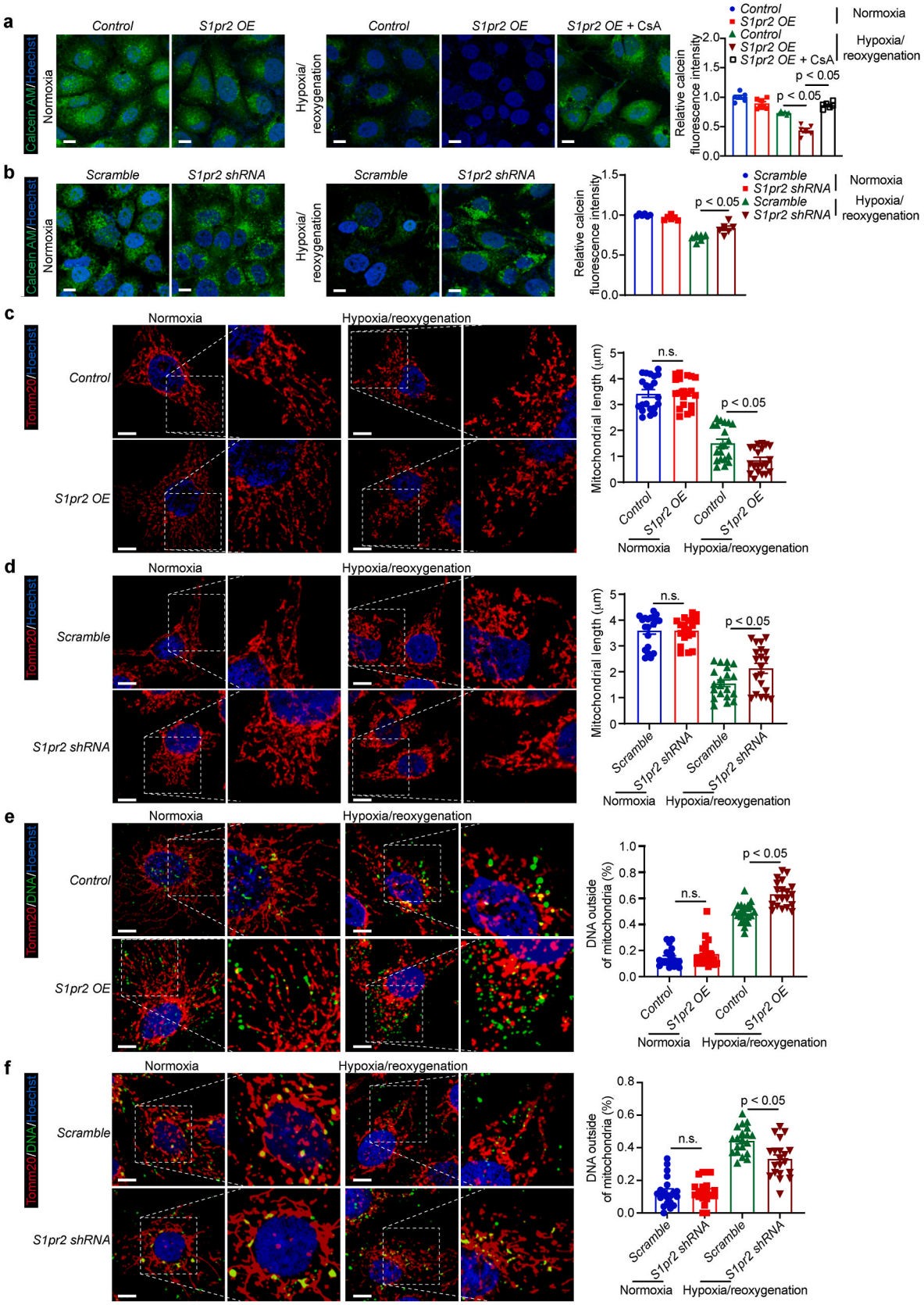

(caption on next page)

Fig. 4. EC-S1PR2 induces excessive mitochondrial fission upon hypoxia/reoxygenation injury. **a** The representative images of calcein acetoxymethyl ester (calcein AM)/$CoCl_2$ staining in CMVECs transfected with *control* and *S1pr2* overexpression plasmids with their quantification to evaluate mitochondrial membrane permeability during H/R (H/R, 6 h of hypoxia/24 h of reoxygenation) (n = 6 per group). **b** The representative images of calcein AM/$CoCl_2$ staining in CMVECs transfected with *scramble* and *S1pr2 shRNA* plasmids with or without Cyclosporin A (CsA) (1 μM), and their quantification to evaluate mitochondrial membrane permeability during H/R (H/R, 6 h of hypoxia/24 h of reoxygenation) (n = 6 per group). **c** The representative images of the Tomm20 staining to visualize mitochondrial morphology in CMVECs transfected with *control* and *S1pr2 overexpression* plasmids with the quantification of mitochondrial length (n = 20 per group). **d** The representative images of the Tomm20 staining to visualize mitochondrial morphology in CMVECs transfected with *scramble* and *S1pr2 shRNA* plasmids with the quantification of mitochondrial length (n = 20 per group). **e** The representative images of co-staining of Tomm20 and mtDNA in CMVECs transfected with *control* and *S1pr2 overexpression* plasmids with their quantification of DNA outside mitochondria (n = 20 per group). **f** The representative images of co-staining of Tomm20 and mtDNA in CMVECs transfected with *scramble* and *S1pr2 shRNA* plasmids by with their quantification of DNA outside mitochondria (n = 20 per group). Data were shown as mean ± SEM. Scale bars: **a**, **b**, **c**, **d**, **e** and **f**, 10 μm. One-way ANOVA (**a**, **b**, **c**, **d**, **e** and **f**).

expression levels of *Gsdmd* in cardiac ECs (Supplementary Fig. 9a). Our *in vivo* data showed that EC-GSDMD knockdown significantly decreased the cardiac infarct size in $S1pr2^{ECTg}$ mice infected with *AAV9-Tie2-Gsdmd shRNA*, in comparison with $S1pr2^{ECTg}$ mice with control *AAV9* vectors (Fig. 7a). Furthermore, EC-specific GSDMD knockdown reversed the enhancing effects of EC-S1PR2 overexpression on the serum LDH levels after cardiac I/R injury (Fig. 7b). As expected, EC-GSDMD knockdown evidently reduced inflammatory factors, including *IL1β*, *IL6*, *IL8*, *IL18* and *TNFα* in $S1pr2^{ECTg}$ mice, while $S1pr2^{ECTg}$ mice infected with control *AAV9* vectors exhibited higher levels of these inflammatory factors (Fig. 7c). Our data further showed that *AAV9-Tie2-Gsdmd* shRNA significantly inhibited excessive neutrophil infiltration and protected cardiomyocytes from cell apoptosis and necrosis after I/R injury in $S1pr2^{ECTg}$ mice (Fig. 7d–e and Supplementary Fig. 9d). *In vitro* data also showed that *Gsdmd* knockdown by *Gsdmd siRNA* significantly reduced cell pyroptosis in *S1pr2*-overexpressing ECs (Supplementary Figs. 9b–c). These data confirmed that EC-S1PR2 was involved in the regulation of EC pyroptosis, which further influenced the extent of heart I/R injury.

3.9. EC-targeted S1PR2 knockdown alleviates cardiac I/R injury in vivo

Since systemic drug administration to modulate S1P receptor signaling is not cell-specific and might have side effects apart from the protective effects on cardiac injuries [46], we thus constructed an EC-specific delivery system via RGD-peptide magnetic nanoparticles to specifically control the expression of S1PR2 in ECs, as previously reported [18,20]. Our results showed that RGD-nanoparticles packaging *S1pr2 siRNA* significantly reduced the expression of *S1pr2*/S1PR2 in cardiac ECs (Fig. 8a–b). RGD-nanoparticles (2.0 mg/kg) were administrated into mice with cardiac I/R injuries. Our results showed that *S1pr2 siRNA* RGD-nanoparticles significantly decreased the cardiac infarct size, with no changes in the ratio of AAR/LV compared with the control mice (Fig. 8c). Furthermore, much lower serum LDH levels were observed in mice treated with *S1pr2 siRNA* nanoparticles (Fig. 8d). Consistently, EC-targeted S1PR2 knockdown resulted in an evident reduction in multiple inflammatory factors, including *IL1β*, *IL6*, *IL8*, *IL18* and *TNFα* (Fig. 8e), and much less neutrophils infiltration in post-I/R myocardium (Fig. 8f). Our further histological analysis revealed much less apoptotic and necrotic cardiomyocytes in mice which received *S1pr2 siRNA* nanoparticles than *scramble* siRNA (Fig. 8g and Supplementary Fig. 10a). Collectively, this study demonstrates that EC-targeted delivery of *S1pr2 siRNA* to inhibit S1PR2 signaling might be a novel therapeutic strategy against cardiac I/R injury.

4. Discussion

Lipidomic analysis provides enormous data and new insight into the pathogenesis of diseases. A previous lipidomic study identified phosphatidylethanolamine lipid products were involved in the process of cerebral ischemia/reperfusion injury [47]. A prospective Finnish cohort study unveiled plasma ceramides, the precursor of complex sphingolipids, can predict cardiovascular death in patients with stable coronary artery disease and acute coronary syndromes [48]. Our lipidomic analysis showed that plasma sphingolipids were significantly decreased after cardiac I/R injury. Further patient plasma showed that plasma S1P concentrations were significantly reduced in the CHD patients after PCI compared to those without PCI operation, suggesting possible involvement of S1P signaling during heart I/R injury. Our observation of reduced plasma S1P levels following cardiac I/R injury and PCI introduces a novel perspective into the dynamics of S1P in the context of cardiac events. We observed a significant decrease in S1P concentrations, which is consistent with Knapp et al.'s observations following myocardial infarction (MI) [24]. Knapp et al.'s study have demonstrated that cardiac infarction markedly reduces plasma S1P levels, associated with decreased levels of S1P and reduced sphingosine kinase activity in platelets [24], indicating that the reduction in plasma S1P is likely due to impaired S1P synthesis in platelets following myocardial infarction. Furthermore, our data indicate that cardiac I/R injury leads to the downregulation of sphingosine kinases in endothelial cells (data not shown). Given that endothelial cells significantly contribute to plasma S1P levels [49], their dysfunction during cardiac I/R injury likely exacerbates the reduction in plasma S1P levels. Although both platelets and endothelial cells may play crucial roles in maintaining plasma S1P levels during heart injuries, there is no direct evidence of a cause-and effect relationship. Further detailed investigations are warranted to fully elucidate the underlying regulatory mechanisms.

Over the past decades, many studies revealed that S1P (or HDL-bound S1P) exhibited cardioprotective properties and particularly protected cardiomyocytes against cell apoptosis [50]. Karliner et al. demonstrated that exogenously supplied S1P, as well as sphingosine kinases (SPHKs) activation by ganglioside GM-1, prevented hypoxia-induced death of neonatal rat cardiomyocytes [51]. It has been reported that the inhibitory effect of S1P on cardiomyocyte apoptosis was mediated via AKT signaling activation [52]. Lecour and colleagues performed *ex vivo* experiments and reported that S1P protected hearts from regional ischemia/reperfusion (I/R) injury [53]. In consistence with these previous studies, our data supported that S1P was an essential bioactive lipid which was involved in the process of cardiac I/R injury.

Extracellular sphingosine 1-phosphate (S1P) exerts multiple biological functions via its distinct S1P receptors (S1PRs) [54]. Each S1P receptor couples to the specific G protein α subunits, triggering various cellular responses [16]. Previous investigations revealed that the S1P–S1PRs signaling pathway played a pivotal role in both physiological and pathological processes in the cardiovascular system [29]. Among the five types of G protein-coupled receptors (S1PR1-S1PR5) for S1P, S1PR1, S1PR2 and S1PR3 are predominantly expressed in cardiovascular system [21]. Previous studies have showed that S1PR1 signaling is essential for the maintenance of vascular endothelial functions and homeostasis [55–57]. Our prior research demonstrated that EC-specific deletion of S1PR1 inhibits the proliferation of reparative $F4/80^{+}Ly6c^{low}$ macrophages, exacerbating pathological cardiac remodeling and worsening cardiac dysfunction following myocardial infarction in mice [21]. This underscores that endothelial S1PR1 exerts protective effects on hearts. However, our present study provides evidences that EC-expressing S1PR2 has a detrimental impact on cardiac I/R injury. These findings suggest that endothelial S1PR1 and S1PR2 have counteracting functions, balancing each other's impacts on cardiac homeostasis and pathology. The precise and detailed interplay between

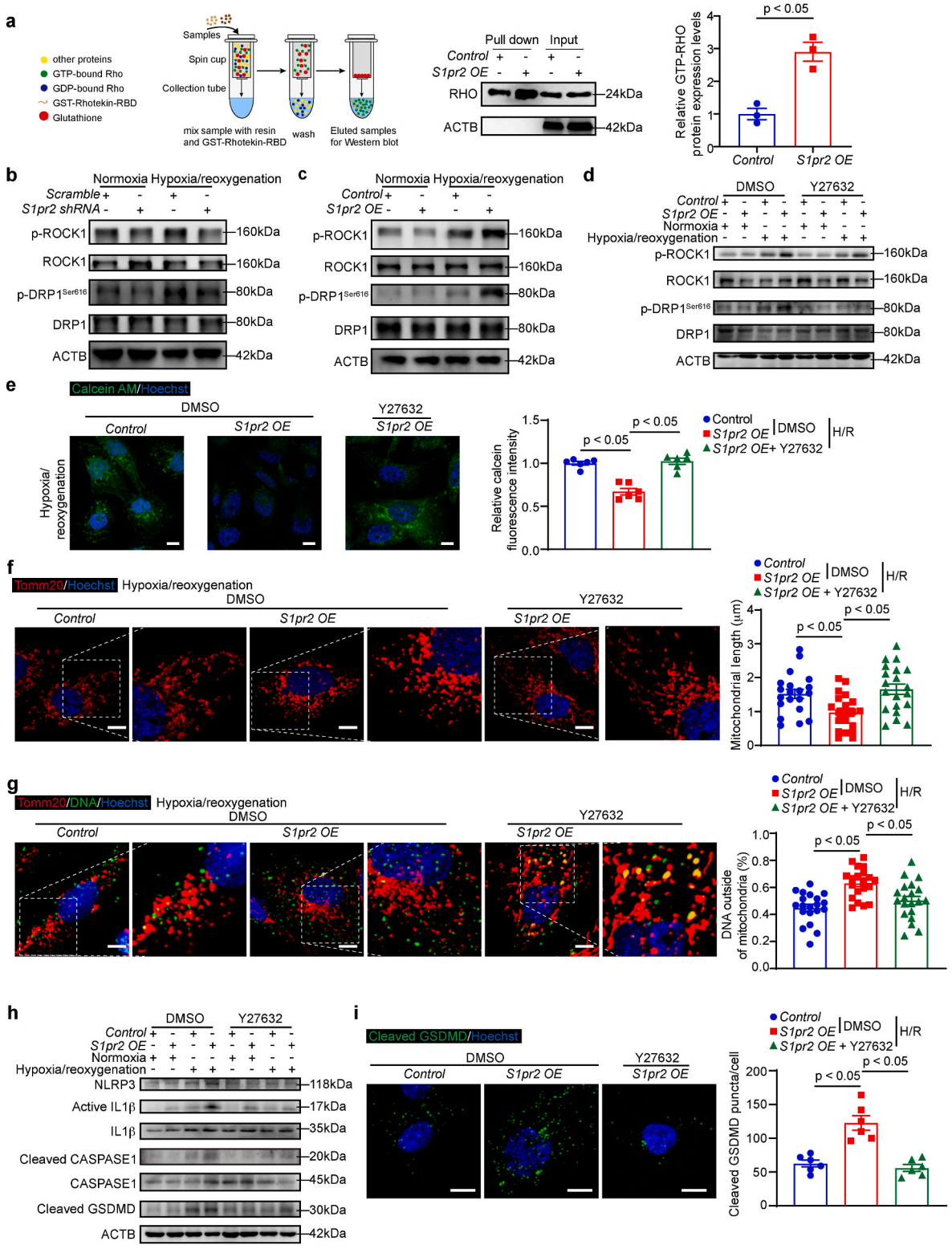

Fig. 5. EC-S1PR2 activates RHO/ROCK1/DRP1 to promote mitochondrial hyperfission, leading to mtDNA release into cytoplasm which triggers NLRP3 inflammasome activation, and subsequently induces endothelial pyroptosis. **a** Schematic diagram showed RHO-GTP pull down assay (the left panel) and western-blotting analysis of RHO protein expression levels (the middle panel) with their quantification (the right panel) (n = 3 per group). **b-d** Western-blotting analysis of the *p*-ROCK1 and *p*-DRP1 expression in the indicated groups. **e** The representative images of calcein AM/$CoCl_2$ staining in CMVECs in indicated groups (n = 6 per group). **f** The representative images of the Tomm20 staining to visualize mitochondrial morphology in CMVECs of indicated groups with the quantification of mitochondrial length (n = 20 per group). **g** The representative images of co-staining of Tomm20 and DNA in CMVECs of indicated groups with their quantification of DNA outside mitochondria (n = 20 per group). **h** Western-blotting analysis of NLRP3, active IL1β, cleaved CASPASE1 and cleaved GSDMD protein expression levels in CMVECs of the indicated groups. **i** The representative images of pyroptosis in CMVECs of the indicated groups (H/R, 6 h of hypoxia/24 h of reoxygenation) by immunofluorescence-staining of cleaved GSDMD (n = 6 per group). Data were shown as mean ± SEM. Scale bars: **e**, **f**, **g** and **i**, 10 μm. Unpaired Student's t-test (**a**). One-way ANOVA (**e**, **f**, **g** and **i**).

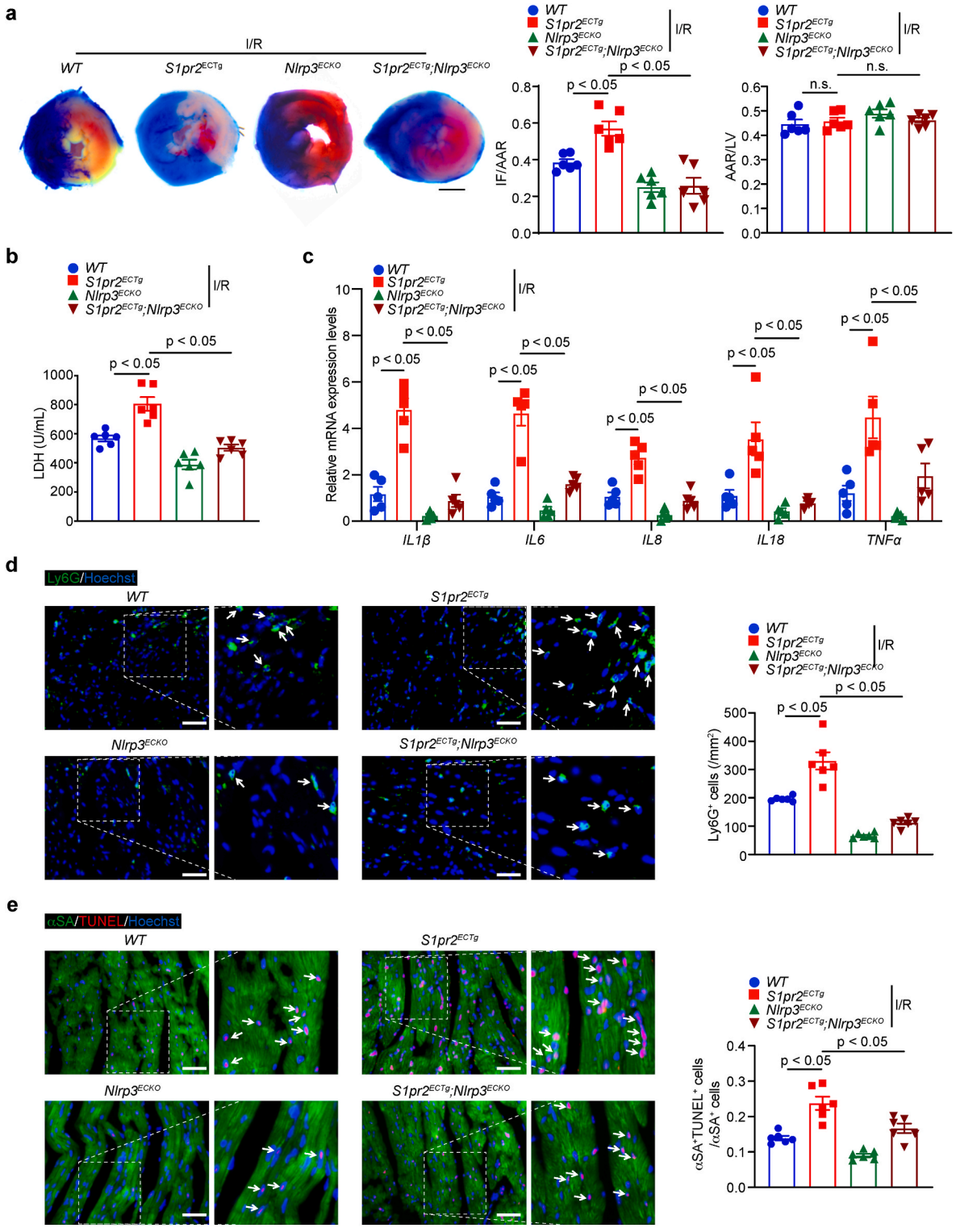

Fig. 6. EC-S1PR2 overexpression aggravates cardiac I/R injury via NLRP3 inflammasome activation. **a** The representative images of evans blue/TTC-staining of heart sections collected from the indicated groups mice after cardiac I/R injury (45 min of ischemia/24 h of reperfusion), with their quantification of the infarct area (IF), at-risk area (AAR), and left ventricle (LV) (n = 6 per group). **b** Serum LDH levels of the indicated groups mice after cardiac I/R injury (45 min of ischemia/24 h of reperfusion) were measured (n = 6 per group). **c** Relative mRNA expression levels of *IL1β*, *IL6*, *IL8*, *IL18* and *TNFα* in heart tissues of the indicated groups mice after cardiac I/R injury (45 min of ischemia/24 h of reperfusion) (n = 5 per group) by RT-qPCR. **d-e** The representative images of immunofluorescence-staining of Ly6G (**d**) and cardiomyocytes apoptosis by co-immunofluorescence-staining of αSA and TUNEL (**e**) in the indicated groups mice after cardiac I/R injury (45 min of ischemia/24 h of reperfusion) (n = 6 per group). Data were shown as mean ± SEM. n.s. indicated not significant. Scale bars: **a**, 2 mm; **d**, **e**, 50 μm. One-way ANOVA (**a**, **b**, **c**, **d** and **e**).

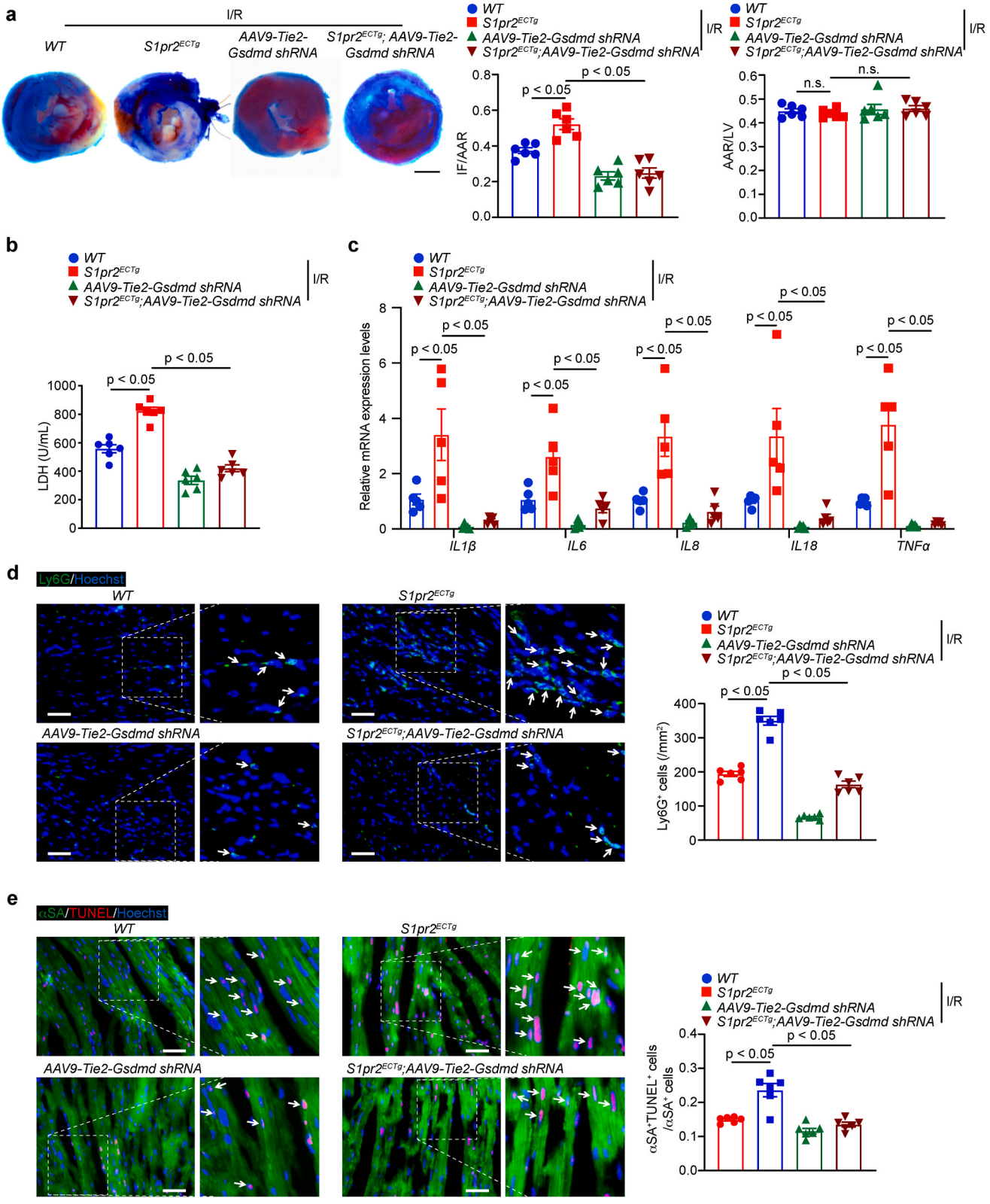

Fig. 7. EC-specific GSDMD knockdown abolishes the detrimental effects of EC-S1PR2 overexpression on cardiac I/R injury *in vivo*. **a** The representative images of evans blue/TTC-staining of heart sections collected from the indicated groups mice after cardiac I/R injury (45 min of ischemia/24 h of reperfusion), with their quantification of the infarct area (IF), at-risk area (AAR), and left ventricle (LV) (n = 6 per group). **b** Serum LDH levels of the indicated groups mice after cardiac I/R injury (45 min of ischemia/24 h of reperfusion) were measured (n = 6 per group). **c** Relative mRNA expression levels of *IL1β*, *IL6*, *IL8*, *IL18* and *TNFα* in heart tissues of the indicated groups mice after cardiac I/R injury (45 min of ischemia/24 h of reperfusion) (n = 5 per group) by RT-qPCR. **d-e** The representative images of immunofluorescence-staining of Ly6G (**d**) and cardiomyocytes apoptosis by co-immunofluorescence-staining of αSA and TUNEL (**e**) in the indicated groups mice after cardiac I/R injury (45 min of ischemia/24 h of reperfusion) (n = 6 per group). Data were shown as mean ± SEM. n.s. indicated not significant. Scale bars: **a**, 2 mm; **d**, **e**, 50 μm. One-way ANOVA (**a**, **b**, **c**, **d** and **e**).

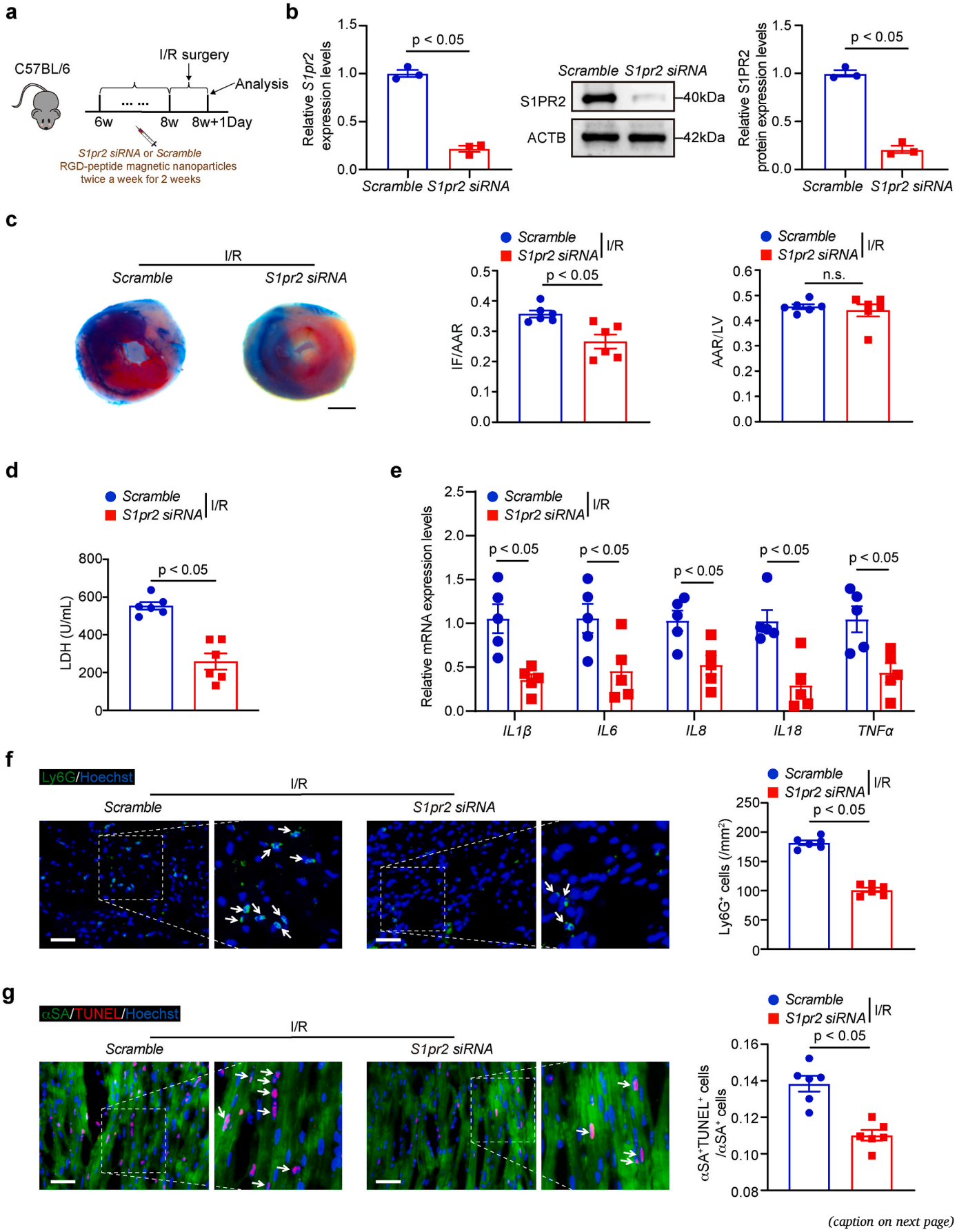

(caption on next page)

Fig. 8. EC-targeted S1PR2 knockdown alleviates cardiac I/R injury *in vivo*. **a-b** Schematic diagram showed the administration of RGD-peptide magnetic nanoparticles (NPs) packaging *S1pr2 siRNA* twice a week for 2 weeks before I/R surgery in mice (**a**), relative mRNA expression levels of *S1pr2* in cardiac ECs administrated with nanoparticles packaging *S1pr2 siRNA* or *scramble* by RT-qPCR and relative S1PR2 protein expression levels by western-blotting (n = 3 per group) (**b**). **c** The representative images of evans blue/TTC-staining of heart sections collected from the indicated groups mice after cardiac I/R injury (45 min of ischemia/24 h of reperfusion), with their quantification of the infarct area (IF), at-risk area (AAR), and left ventricle (LV) (n = 6 per group). **d** Serum LDH levels of the indicated groups mice after cardiac I/R injury (45 min of ischemia/24 h of reperfusion) were measured (n = 6 per group). **e** Relative mRNA expression levels of *IL1β*, *IL6*, *IL8*, *IL18* and *TNFα* in heart tissues of the indicated groups mice after cardiac I/R injury (45 min of ischemia/24 h of reperfusion) (n = 5 per group) by RT-qPCR. **f-g** The representative images of immunofluorescence-staining of Ly6G (**f**) and cardiomyocytes apoptosis by co-immunofluorescence-staining of αSA and TUNEL (**g**) in the indicated groups mice after cardiac I/R injury (45 min of ischemia/24 h of reperfusion) (n = 6 per group). Data were shown as mean ± SEM. n.s. indicated not significant. Scale bars: **c**, 2 mm; **f**, **g**, 50 μm. Unpaired Student's t-test (**b**, **c**, **d**, **e**, **f** and **g**).

S1PR1 and S1PR2 warrants further investigation to elucidate the intricate mechanisms underlying cardiovascular homeostasis.

Previous studies have established that S1P facilitated Akt activation in adult WT cardiomyocytes, but not in S1PR2$^{-/-}$ or S1PR3$^{-/-}$ cardiomyocytes, suggesting that both CM-S1PR2 and S1PR3 regulate Akt activity, which is essential for CM survival [31]. In consistence with this report, our *in vitro* experiments showed that CM-expressing S1PR2 enhanced cell survival following hypoxia-reoxygenation injury. Conversely, we observed that EC-expressing S1PR2 had a deleterious impact on CM survival upon H/R injury *in vitro*. These results suggest that while CM-S1PR2 exerts protective effects on cardiomyocytes, the deleterious impacts of EC-S1PR2 could mask the specific cellular role of S1PR2. This observation may explain why mice completely lacking *S1pr2* exhibited similar infarct sizes to WT mice in I/R mode [31]. In this study, we took advantage of both EC-specific *S1pr2* loss-of-function and gain-of-function mice in a cardiac I/R injury model. Our *in vivo* data showed that S1PR2 deletion in ECs ameliorated cardiac I/R injury and diminished inflammatory responses, whereas EC-S1PR2 gain--of-function promoted inflammation and aggravated I/R-induced infarct. Our study provides direct *in vivo* evidence that EC-expressing S1PR2 played a pivotal role in the regulation of cardiac I/R injury.

Cell mitochondrial dynamic balance is essential for the maintenance of endothelial functions and homeostasis [58]. In addition to the roles of mitochondria in energy metabolism, mitochondria serves as sensors for environmental stress and regulates cellular responses [59]. Mitochondrial damage can lead to endothelial dysfunction and aggravate cardiac I/R injury [60]. Our investigation revealed that EC-S1PR2 aggravated I/R-induced EC mitochondria hyperfission and impaired mitochondrial dynamics. As far as we acknowledge, our investigations first revealed that S1PR2 played an essential role in the regulation of mitochondria dynamics in ECs subjected to I/R injury, implying the key role of EC mitochondria homeostasis for cardiac I/R injury.

It has been shown that mitochondrial fission and subsequent fragmentation occurs in cardiac cells during cardiac I/R injury [61]. This process of mitochondrial fission is mediated by a key regulator, DRP1, which recruits to mitochondrial surface and further facilitates mitochondrial scission [62]. Under pathological conditions, the hyperactivation of DRP1 can result in an excessive mitochondrial fission, impairing mitochondrial function and structural integrity [63]. This excessive mitochondrial fission can further lead to the release of mitochondrial DNA (mtDNA) into the cytoplasm, triggering innate immune responses [64]. Previous studies showed that DRP1 activation is regulated by its upstream RHO-associated coiled-coil kinase 1 (ROCK1) signaling pathway [65,66]. Activation of ROCK1 by phosphorylation can promote DRP1 activity and thus elicit mitochondrial hyperfission [63]. Previous studies reveal that S1PR2 can activate the ROCK1 signaling pathway via RHO-GTP in various cell types [42,67]. In consistent with previous studies [42,67], our investigations indicated that S1PR2 activated RHO/ROCK1 signaling pathway in ECs, and further triggered the activation of DRP1 signaling pathway, which led to the mitochondria hyperfission and thus resulted in mtDNA leakage into cytoplasm. Our study highlights that S1PR2/RHO/ROCK1/DRP1 signaling activation leads to mitochondrial damage, which exerts the harmful effects on cardiac I/R injury, suggesting that pharmacological target against S1PR2/RHO/ROCK1/DRP1 pathway might be a novel treatment to protect against cardiac I/R injury via maintenance of mitochondrial homeostasis.

As previously reported, the extracellular release of mtDNA can elicit a potent activation of NLRP3 inflammasome, thereby triggering the activation of CASPASE-1 and the subsequent release of proinflammatory cytokines, including interleukin 1 (IL1) and interleukin 18 (IL18) [13]. Consistently, our experiments showed that S1PR2 triggered NLRP3 inflammasome activation in cardiac ECs after I/R injury and that EC-specific *Nlrp3* deletion reversed the enhancing effect of EC-S1PR2 overexpression on cardiac I/R injury *in vivo*, suggesting a key role of S1PR2 for EC inflammasome activation and its influences on cardiac I/R injury. Concurrently, inflammasome activation triggers a distinct form of inflammatory cell death, referred to as pyroptosis [14]. Pyroptosis is characterized by the proteolytic cleavage of gasdermin D (GSDMD) by CASPASE-1, which results in the formation of pores within the cellular membrane, thereby disrupting cell membrane, and ultimately causes cell death [68]. This intricate interplay between inflammasome activation and pyroptosis has been shown to exert an essential role in the pathophysiology of cardiovascular diseases, including atherosclerosis, myocardial infarction, cardiac hypertrophy, abdominal aortic aneurysm and arrhythmia [69,70]. However, whether endothelial inflammasome activation and pyroptosis are involved in the pathological process of cardiac I/R injury has not been clarified yet. In our study, we showed EC-S1PR2 triggered NLRP3 inflammasome activation upon cardiac I/R injury, and further led to cell pyroptosis, which contributed to the deleterious effects on cardiac I/R injury. Our study offers a new insight into endothelial inflammasome activation and pyroptosis as a key regulator during cardiac I/R injury, potentially leading to novel therapeutic interventions for I/R injury via suppressing NLRP3 inflammasome activation and cell pyroptosis.

We constructed an EC-targeted delivery system of *S1pr2 siRNA* via RGD-Fe_3O_4 nanoparticles, which achieves a high efficiency of EC-specific *S1pr2* knockdown *in vivo*. RGD-nanoparticles packaging *S1pr2-siRNA* to specifically knockdown *S1pr2* in ECs significantly ameliorate cardiac I/R injury, therefore providing a promising cell-targeted therapy for myocardial infarction and subsequent reperfusion injury. However, we recognize the limitation of this approach in clinical settings, where the unpredictable nature of ischemic events makes pretreatment almost impractical. This limitation poses a significant barrier to the direct translation of our findings into clinical practice. To address this issue, we will explore strategies for the rapid administration of nanoparticles immediately following the onset of ischemic events in future research. Such approaches could pave the way for the effective integration of nanoparticle-based therapies into the treatment regimen for cardiac I/R injury.

Taken together, our investigations identified EC-S1PR2 as a key regulator to control inflammatory responses and cardiac I/R injury. EC-specific *S1pr2* loss-of-function significantly reduced inflammatory responses and cardiac I/R injury, while EC-specific *S1pr2* gain-of-function aggravated cardiac I/R injury. Mechanistically, S1P–S1PR2 signaling activates RHO/ROCK1/DRP1 pathways to induce EC mitochondrial hyperfission, leading to mtDNA release into cytoplasm, which results in NLRP3 inflammasome activation and subsequently induces cell pyroptosis, and thus aggravates cardiac I/R-induced inflammatory responses and heart injury (Supplementary Fig. 11). Furthermore, we constructed

RGD-peptide magnetic nanoparticles packaging *S1pr2-siRNA* to specifically knockdown S1PR2 in ECs, which significantly ameliorated cardiac I/R injuries *in vivo*, providing a future promising EC-target therapy for cardiac I/R injury through S1PR2 signal pathway.

Funding

The study was supported by funds from the National Key Research and Development Program of China (2019YFA0801502, 2022YFA1104503), the National Natural Science Foundation of China (82170257, 82270395, 82370280, 82170477), Science and Technology Commission of Shanghai Municipality (21ZR1440900), and Key Disciplines Group Construction Project of Shanghai Pudong New Area Health Commission (Grant No. PWZxq2022-02).

CRediT authorship contribution statement

Yunhao Duan: Visualization, Validation, Methodology, Data curation. **Qinyu Li:** Methodology, Data curation. **Jinjin Wu:** Resources, Project administration, Investigation. **Caixia Zhou:** Formal analysis. **Xiuxiang Liu:** Formal analysis. **Jinnan Yue:** Methodology. **Xiaoli Chen:** Project administration. **Jie Liu:** Supervision. **Qi Zhang:** Project administration. **Yuzhen Zhang:** Supervision. **Lin Zhang:** Writing – review & editing, Writing – original draft, Supervision, Project administration, Funding acquisition, Conceptualization.

Declaration of competing interest

The authors read and understood the Redox Biology's policy on declaration of interests and declare the following:

The authors declare no competing financial interests in this manuscript entitled "A detrimental role of endothelial S1PR2 in cardiac ischemia-reperfusion injury via modulating mitochondrial dysfunction, NLRP3 inflammasome activation, and pyroptosis".

Data availability

Data will be made available on request.

Acknowledgements

We thank the staff members of the Integrated Laser Microscopy System at the National Facility for Protein Science in Shanghai (NFPS), Shanghai Advanced Research Institute, Chinese Academy of Sciences, China for sample preparation, data collection and analysis.

Appendix A. Supplementary data

Supplementary data to this article can be found online at https://doi.org/10.1016/j.redox.2024.103244.

References

[1] D.M. Yellon, D.J. Hausenloy, Myocardial reperfusion injury, N. Engl. J. Med. 357 (2007) 1121–1135, https://doi.org/10.1056/NEJMra071667.
[2] S.M. Davidson, et al., Multitarget strategies to reduce myocardial ischemia/reperfusion injury: JACC review Topic of the Week, J. Am. Coll. Cardiol. 73 (2019) 89–99, https://doi.org/10.1016/j.jacc.2018.09.086.
[3] J. Wang, S. Toan, H. Zhou, Mitochondrial quality control in cardiac microvascular ischemia-reperfusion injury: new insights into the mechanisms and therapeutic potentials, Pharmacol. Res. 156 (2020) 104771, https://doi.org/10.1016/j.phrs.2020.104771.
[4] T. Scarabelli, et al., Apoptosis of endothelial cells precedes myocyte cell apoptosis in ischemia/reperfusion injury, Circulation 104 (2001) 253–256, https://doi.org/10.1161/01.cir.104.3.253.
[5] T. Gori, et al., Sildenafil prevents endothelial dysfunction induced by ischemia and reperfusion via opening of adenosine triphosphate-sensitive potassium channels: a human in vivo study, Circulation 111 (2005) 742–746, https://doi.org/10.1161/01.cir.0000155252.23933.2d.
[6] M.B. Forman, R. Virmani, D.W. Puett, Mechanisms and therapy of myocardial reperfusion injury, Circulation 81 (1990) IV69–78.
[7] M.B. Forman, D.W. Puett, R. Virmani, Endothelial and myocardial injury during ischemia and reperfusion: pathogenesis and therapeutic implications, J. Am. Coll. Cardiol. 13 (1989) 450–459, https://doi.org/10.1016/0735-1097(89)90526-3.
[8] X. Chang, et al., Coronary microvascular injury in myocardial infarction: perception and knowledge for mitochondrial quality control, Theranostics 11 (2021) 6766–6785, https://doi.org/10.7150/thno.60143.
[9] S.B. Ong, D.J. Hausenloy, Mitochondrial morphology and cardiovascular disease, Cardiovasc. Res. 88 (2010) 16–29, https://doi.org/10.1093/cvr/cvq237.
[10] S.B. Ong, et al., Inhibiting mitochondrial fission protects the heart against ischemia/reperfusion injury, Circulation 121 (2010) 2012–2022, https://doi.org/10.1161/circulationaha.109.906610.
[11] P. Pérez-Treviño, M. Velásquez, N. García, Mechanisms of mitochondrial DNA escape and its relationship with different metabolic diseases, Biochimica et biophysica acta. Molecular basis of disease 1866 (2020) 165761, https://doi.org/10.1016/j.bbadis.2020.165761.
[12] R.J. Youle, M. Karbowski, Mitochondrial fission in apoptosis, Nat. Rev. Mol. Cell Biol. 6 (2005) 657–663, https://doi.org/10.1038/nrm1697.
[13] A.T. Moehlman, R.J. Youle, Mitochondrial quality control and Restraining innate Immunity, Annu. Rev. Cell Dev. Biol. 36 (2020) 265–289, https://doi.org/10.1146/annurev-cellbio-021820-101354.
[14] J. Zhang, S. Wirtz, Does pyroptosis play a role in inflammasome-related disorders? Int. J. Mol. Sci. 23 (2022) https://doi.org/10.3390/ijms231810453.
[15] R.L. Proia, T. Hla, Emerging biology of sphingosine-1-phosphate: its role in pathogenesis and therapy, The Journal of clinical investigation 125 (2015) 1379–1387, https://doi.org/10.1172/jci76369.
[16] M. Maceyka, K.B. Harikumar, S. Milstien, S. Spiegel, Sphingosine-1-phosphate signaling and its role in disease, Trends Cell Biol. 22 (2012) 50–60, https://doi.org/10.1016/j.tcb.2011.09.003.
[17] X. Liu, et al., Endothelial S1pr1 regulates pressure overload-induced cardiac remodelling through AKT-eNOS pathway, J. Cell Mol. Med. 24 (2020) 2013–2026, https://doi.org/10.1111/jcmm.14900.
[18] C. Zhou, et al., Endothelial S1pr2 regulates post-ischemic angiogenesis via AKT/eNOS signaling pathway, Theranostics 12 (2022) 5172–5188, https://doi.org/10.7150/thno.71585.
[19] T. Zhuang, et al., Endothelial Foxp1 Suppresses atherosclerosis via modulation of Nlrp3 inflammasome activation, Circ. Res. 125 (2019) 590–605, https://doi.org/10.1161/CIRCRESAHA.118.314402.
[20] J. Pi, et al., A MicroRNA302-367-Erk1/2-Klf2-S1pr1 pathway prevents Tumor growth via restricting angiogenesis and improving vascular Stability, Circ. Res. 120 (2017) 85–98, https://doi.org/10.1161/circresaha.116.309757.
[21] Y. Kuang, et al., Vascular endothelial S1pr1 ameliorates adverse cardiac remodelling via stimulating reparative macrophage proliferation after myocardial infarction, Cardiovasc. Res. 117 (2021) 585–599, https://doi.org/10.1093/cvr/cvaa046.
[22] J. Liu, et al., Endothelial forkhead box transcription factor P1 regulates pathological cardiac remodeling through transforming growth factor-beta1-endothelin-1 signal pathway, Circulation 140 (2019) 665–680, https://doi.org/10.1161/CIRCULATIONAHA.119.039767.
[23] A.J. Valente, L.A. Maddalena, E.L. Robb, F. Moradi, J.A. Stuart, A simple ImageJ macro tool for analyzing mitochondrial network morphology in mammalian cell culture, Acta Histochem. 119 (2017) 315–326, https://doi.org/10.1016/j.acthis.2017.03.001.
[24] M. Knapp, et al., Myocardial infarction differentially alters sphingolipid levels in plasma, erythrocytes and platelets of the rat, Basic Res. Cardiol. 107 (2012) 294, https://doi.org/10.1007/s00395-012-0294-0.
[25] M. Knapp, et al., Plasma sphingosine-1-phosphate concentration is reduced in patients with myocardial infarction, Med Sci Monit 15 (2009) CR490–493.
[26] S. Morel, et al., Sphingosine-1-phosphate reduces ischaemia-reperfusion injury by phosphorylating the gap junction protein Connexin43, Cardiovasc. Res. 109 (2016) 385–396, https://doi.org/10.1093/cvr/cvw004.
[27] G. Theilmeier, et al., High-density lipoproteins and their constituent, sphingosine-1-phosphate, directly protect the heart against ischemia/reperfusion injury in vivo via the S1P3 lysophospholipid receptor, Circulation 114 (2006) 1403–1409, https://doi.org/10.1161/CIRCULATIONAHA.105.607135.
[28] A. Cannavo, et al., beta(1)-Blockade prevents post-ischemic myocardial decompensation via beta(3)AR-dependent protective sphingosine-1 phosphate signaling, J. Am. Coll. Cardiol. 70 (2017) 182–192, https://doi.org/10.1016/j.jacc.2017.05.020.
[29] C.K. Means, J.H. Brown, Sphingosine-1-phosphate receptor signalling in the heart, Cardiovasc. Res. 82 (2009) 193–200, https://doi.org/10.1093/cvr/cvp086.
[30] J.D. Saba, T. Hla, Point-counterpoint of sphingosine 1-phosphate metabolism, Circ. Res. 94 (2004) 724–734, https://doi.org/10.1161/01.RES.0000122383.60368.24.
[31] C.K. Means, et al., Sphingosine 1-phosphate S1P2 and S1P3 receptor-mediated Akt activation protects against in vivo myocardial ischemia-reperfusion injury, Am. J. Physiol. Heart Circ. Physiol. 292 (2007) H2944–H2951, https://doi.org/10.1152/ajpheart.01331.2006.
[32] K. Wang, et al., Structural mechanism for GSDMD targeting by Autoprocessed caspases in pyroptosis, Cell 180 (2020) 941–955 e920, https://doi.org/10.1016/j.cell.2020.02.002.
[33] J. Shi, et al., Cleavage of GSDMD by inflammatory caspases determines pyroptotic cell death, Nature 526 (2015) 660–665, https://doi.org/10.1038/nature15514.
[34] H. Xi, et al., Caspase-1 inflammasome activation Mediates homocysteine-induced pyrop-apoptosis in endothelial cells, Circ. Res. 118 (2016) 1525–1539, https://doi.org/10.1161/CIRCRESAHA.116.308501.

[35] R. Zhou, A.S. Yazdi, P. Menu, J. Tschopp, A role for mitochondria in NLRP3 inflammasome activation, Nature 469 (2011) 221–225, https://doi.org/10.1038/nature09663.
[36] Y. Han, et al., SIRT1 agonism modulates cardiac NLRP3 inflammasome through pyruvate dehydrogenase during ischemia and reperfusion, Redox Biol. 34 (2020) 101538, https://doi.org/10.1016/j.redox.2020.101538.
[37] M. Panel, et al., Small-molecule inhibitors of cyclophilins block opening of the mitochondrial permeability transition pore and protect mice from hepatic ischemia/reperfusion injury, Gastroenterology 157 (2019) 1368–1382, https://doi.org/10.1053/j.gastro.2019.07.026.
[38] R.M. Bell, et al., Matrix metalloproteinase inhibition protects CyPD knockout mice independently of RISK/mPTP signalling: a parallel pathway to protection, Basic Res. Cardiol. 108 (2013) 331, https://doi.org/10.1007/s00395-013-0331-7.
[39] Q. Zhang, et al., STING signaling sensing of DRP1-dependent mtDNA release in kupffer cells contributes to lipopolysaccharide-induced liver injury in mice, Redox Biol. 54 (2022) 102367, https://doi.org/10.1016/j.redox.2022.102367.
[40] S. Park, et al., Defective mitochondrial fission augments NLRP3 inflammasome activation, Sci. Rep. 5 (2015) 15489, https://doi.org/10.1038/srep15489.
[41] G. Zhang, et al., Critical role of sphingosine-1-phosphate receptor 2 (S1PR2) in acute vascular inflammation, Blood 122 (2013) 443–455, https://doi.org/10.1182/blood-2012-11-467191.
[42] T. Sanchez, et al., Induction of vascular permeability by the sphingosine-1-phosphate receptor-2 (S1P2R) and its downstream effectors ROCK and PTEN, Arterioscler. Thromb. Vasc. Biol. 27 (2007) 1312–1318, https://doi.org/10.1161/ATVBAHA.107.143735.
[43] H. Shimokawa, S. Sunamura, K. Satoh, RhoA/rho-kinase in the cardiovascular system, Circ. Res. 118 (2016) 352–366, https://doi.org/10.1161/CIRCRESAHA.115.306532.
[44] Q. Zhang, et al., ROCK1 induces dopaminergic nerve cell apoptosis via the activation of Drp1-mediated aberrant mitochondrial fission in Parkinson's disease, Exp. Mol. Med. 51 (2019) 1–13, https://doi.org/10.1038/s12276-019-0318-z.
[45] W. Wang, et al., Mitochondrial fission triggered by hyperglycemia is mediated by ROCK1 activation in podocytes and endothelial cells, Cell Metab 15 (2012) 186–200, https://doi.org/10.1016/j.cmet.2012.01.009.
[46] S. Flemming, et al., Sphingosine-1-Phosphate receptor-1 agonist Sew2871 causes severe cardiac side effects and does not improve microvascular barrier breakdown in sepsis, Shock 49 (2018) 71–81, https://doi.org/10.1097/SHK.0000000000000908.
[47] Q.Z. Tuo, et al., Thrombin induces ACSL4-dependent ferroptosis during cerebral ischemia/reperfusion, Signal Transduct. Targeted Ther. 7 (2022) 59, https://doi.org/10.1038/s41392-022-00917-z.
[48] R. Laaksonen, et al., Plasma ceramides predict cardiovascular death in patients with stable coronary artery disease and acute coronary syndromes beyond LDL-cholesterol, Eur. Heart J. 37 (2016) 1967–1976, https://doi.org/10.1093/eurheartj/ehw148.
[49] K. Venkataraman, et al., Vascular endothelium as a contributor of plasma sphingosine 1-phosphate, Circ. Res. 102 (2008) 669–676, https://doi.org/10.1161/circresaha.107.165845.
[50] E. Jozefczuk, T.J. Guzik, M. Siedlinski, Significance of sphingosine-1-phosphate in cardiovascular physiology and pathology, Pharmacol. Res. 156 (2020) 104793, https://doi.org/10.1016/j.phrs.2020.104793.
[51] J.S. Karliner, N. Honbo, K. Summers, M.O. Gray, E.J. Goetzl, The lysophospholipids sphingosine-1-phosphate and lysophosphatidic acid enhance survival during hypoxia in neonatal rat cardiac myocytes, Journal of molecular and cellular cardiology 33 (2001) 1713–1717, https://doi.org/10.1006/jmcc.2001.1429.
[52] J. Zhang, et al., Signals from type 1 sphingosine 1-phosphate receptors enhance adult mouse cardiac myocyte survival during hypoxia, Am. J. Physiol. Heart Circ. Physiol. 293 (2007) H3150–H3158, https://doi.org/10.1152/ajpheart.00587.2006.
[53] S. Lecour, et al., Identification of a novel role for sphingolipid signaling in TNF alpha and ischemic preconditioning mediated cardioprotection, Journal of molecular and cellular cardiology 34 (2002) 509–518, https://doi.org/10.1006/jmcc.2002.1533.
[54] S. Spiegel, S. Milstien, Sphingosine-1-phosphate: an enigmatic signalling lipid, Nat. Rev. Mol. Cell Biol. 4 (2003) 397–407, https://doi.org/10.1038/nrm1103.
[55] Y. Xiong, T. Hla, S1P control of endothelial integrity, Curr. Top. Microbiol. Immunol. 378 (2014) 85–105, https://doi.org/10.1007/978-3-319-05879-5_4.
[56] M.J. Lee, et al., Vascular endothelial cell adherens junction assembly and morphogenesis induced by sphingosine-1-phosphate, Cell 99 (1999) 301–312, https://doi.org/10.1016/s0092-8674(00)81661-x.
[57] J.G. Garcia, et al., Sphingosine 1-phosphate promotes endothelial cell barrier integrity by Edg-dependent cytoskeletal rearrangement, The Journal of clinical investigation 108 (2001) 689–701, https://doi.org/10.1172/jci12450.
[58] M.A. Kluge, J.L. Fetterman, J.A. Vita, Mitochondria and endothelial function, Circ. Res. 112 (2013) 1171–1188, https://doi.org/10.1161/circresaha.111.300233.
[59] S. Caja, J.A. Enríquez, Mitochondria in endothelial cells: sensors and integrators of environmental cues, Redox Biol. 12 (2017) 821–827, https://doi.org/10.1016/j.redox.2017.04.021.
[60] X.G. Guo, et al., Mapping and ablation of anteroseptal atrial tachycardia in patients with congenitally corrected transposition of the great arteries: implication of pulmonary sinus cusps, Europace : European pacing, arrhythmias, and cardiac electrophysiology : journal of the working groups on cardiac pacing, arrhythmias, and cardiac cellular electrophysiology of the European Society of Cardiology 19 (2017) 2015–2022, https://doi.org/10.1093/europace/euw281.
[61] C. Maneechote, et al., Differential temporal therapies with pharmacologically targeted mitochondrial fission/fusion protect the brain against acute myocardial ischemia-reperfusion injury in prediabetic rats: the crosstalk between mitochondrial apoptosis and inflammation, Eur. J. Pharmacol. 956 (2023) 175939, https://doi.org/10.1016/j.ejphar.2023.175939.
[62] J.M. Quiles, B. Gustafsson A, The role of mitochondrial fission in cardiovascular health and disease, Nat. Rev. Cardiol. 19 (2022) 723–736, https://doi.org/10.1038/s41569-022-00703-y.
[63] S. Miwa, S. Kashyap, E. Chini, T. von Zglinicki, Mitochondrial dysfunction in cell senescence and aging, The Journal of clinical investigation 132 (2022), https://doi.org/10.1172/jci158447.
[64] A.P. West, G.S. Shadel, Mitochondrial DNA in innate immune responses and inflammatory pathology, Nat. Rev. Immunol. 17 (2017) 363–375, https://doi.org/10.1038/nri.2017.21.
[65] C. Qu, et al., RhoA/ROCK signaling regulates drp1-mediated mitochondrial fission during collective cell migration, Front. Cell Dev. Biol. 10 (2022) 882581, https://doi.org/10.3389/fcell.2022.882581.
[66] C.S. Brand, V.P. Tan, J.H. Brown, S. Miyamoto, RhoA regulates Drp1 mediated mitochondrial fission through ROCK to protect cardiomyocytes, Cell. Signal. 50 (2018) 48–57, https://doi.org/10.1016/j.cellsig.2018.06.012.
[67] C.R. Panta, et al., Sphingosine-1-Phosphate enhances α(1)-adrenergic vasoconstriction via S1P2-G(12/13)-ROCK mediated signaling, Int. J. Mol. Sci. 20 (2019), https://doi.org/10.3390/ijms20246361.
[68] S.S. Faria, et al., Induction of pyroptotic cell death as a potential tool for cancer treatment, Journal of inflammation (London, England) 19 (2022) 19, https://doi.org/10.1186/s12950-022-00316-9.
[69] X. Chen, P.C. Tian, K. Wang, M. Wang, K. Wang, Pyroptosis: role and mechanisms in cardiovascular disease, Frontiers in cardiovascular medicine 9 (2022) 897815, https://doi.org/10.3389/fcvm.2022.897815.
[70] M. Wortmann, et al., Necrotic cell debris induces a NF-κB-driven inflammasome response in vascular smooth muscle cells derived from abdominal aortic aneurysms (AAA-SMC), Biochemical and biophysical research communications 511 (2019) 343–349, https://doi.org/10.1016/j.bbrc.2019.02.051.